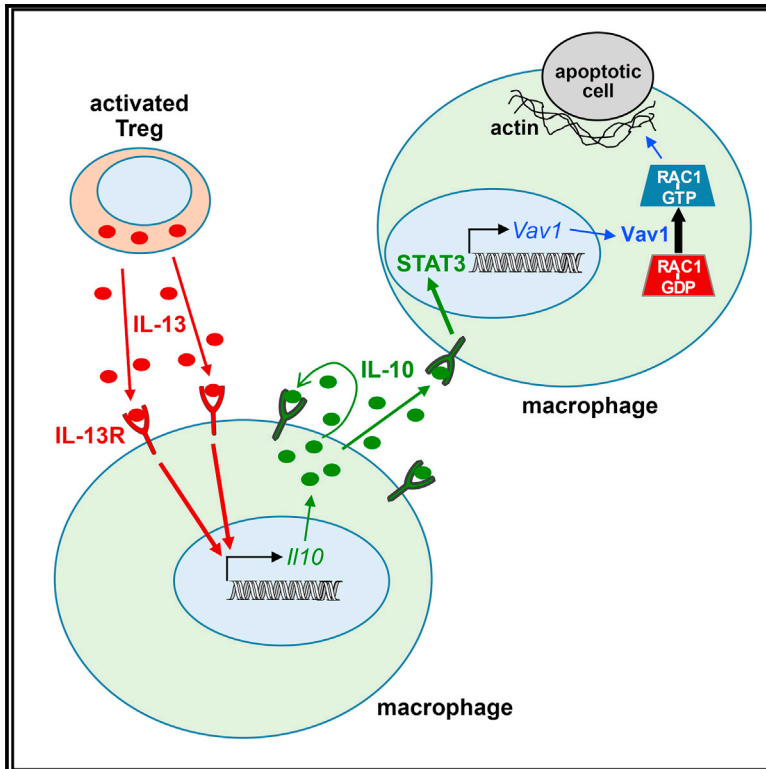


Immunity

Regulatory T Cells Promote Macrophage Efferocytosis during Inflammation Resolution

Graphical Abstract



Authors

Jonathan D. Proto, Amanda C. Doran, Galina Gusarova, ..., George Kuriakose, Jahar Bhattacharya, Ira Tabas

Correspondence

iat1@columbia.edu

In Brief

Regulatory T cells suppress inflammation and promote tissue repair in multiple contexts. Proto, Doran, et al. show that Treg cells enhance the ability of macrophages to engulf apoptotic cells (efferocytosis) and thereby promote resolution of inflammation.

Highlights

- Depletion of Treg cells impairs efferocytosis during inflammation resolution
- Treg cell transfer to mice with atherosclerosis improves lesional efferocytosis
- Treg cells secrete IL-13, which stimulates IL-10 production in macrophages
- Macrophage IL-10 induces Vav1, which activates Rac1 and apoptotic cell engulfment

Regulatory T Cells Promote Macrophage Efferocytosis during Inflammation Resolution

Jonathan D. Proto,^{1,5,7} Amanda C. Doran,^{1,7} Galina Gusarova,¹ Arif Yurdagul, Jr.,¹ Erdi Sozen,^{1,4} Manikandan Subramanian,^{1,6} Mohammad N. Islam,¹ Christina C. Rymond,¹ Jasper Du,¹ Jaime Hook,¹ George Kuriakose,¹ Jahar Bhattacharya,^{1,2} and Ira Tabas^{1,2,3,8,*}

¹Department of Medicine, Columbia University, New York, NY 10032, USA

²Department of Physiology and Cellular Biophysics, Columbia University, New York, NY 10032, USA

³Department of Pathology and Cell Biology, Columbia University, New York, NY 10032, USA

⁴Department of Biochemistry, Marmara University, Istanbul, Turkey

⁵Present address: Sanofi, Framingham, MA, USA

⁶Present address: CSIR-Institute of Genomics and Integrative Biology, New Delhi, India

⁷These authors contributed equally

⁸Lead Contact

*Correspondence: iat1@columbia.edu

<https://doi.org/10.1016/j.immuni.2018.07.015>

SUMMARY

Regulatory T (Treg) cell responses and apoptotic cell clearance (efferocytosis) represent critical arms of the inflammation resolution response. We sought to determine whether these processes might be linked through Treg-cell-mediated enhancement of efferocytosis. In zymosan-induced peritonitis and lipopolysaccharide-induced lung injury, Treg cells increased early in resolution, and Treg cell depletion decreased efferocytosis. In advanced atherosclerosis, where defective efferocytosis drives disease progression, Treg cell expansion improved efferocytosis. Mechanistic studies revealed the following sequence: (1) Treg cells secreted interleukin-13 (IL-13), which stimulated IL-10 production in macrophages; (2) autocrine-paracrine signaling by IL-10 induced Vav1 in macrophages; and (3) Vav1 activated Rac1 to promote apoptotic cell engulfment. In summary, Treg cells promote macrophage efferocytosis during inflammation resolution via a transcellular signaling pathway that enhances apoptotic cell internalization. These findings suggest an expanded role of Treg cells in inflammation resolution and provide a mechanistic basis for Treg-cell-enhancement strategies for non-resolving inflammatory diseases.

INTRODUCTION

A program known as inflammation resolution dampens inflammation and promotes tissue repair during and after the host response to pathogens and tissue injury (Buckley et al., 2014). Resolution is mediated by protein and lipid mediators secreted by inflammatory cells. These mediators bind specific receptors on effector cells, notably leukocytes and myofibroblasts, leading to the activation of various resolution and repair pathways. A key

process in the resolution response is the phagocytosis of apoptotic cells, known as efferocytosis, which prevents apoptotic cells from becoming necrotic and pro-inflammatory (Godson et al., 2000; Buckley et al., 2014; Arandjelovic and Ravichandran, 2015). Pro-resolving mediators have been shown to promote efferocytosis in cultured macrophages and in a variety of disease models *in vivo*, including acute peritonitis, lung injury, and atherosclerosis (Serhan et al., 2014). Moreover, signaling through certain efferocytosis receptors can inhibit inflammatory signaling pathways and promote the secretion of resolution mediators (Fadok et al., 1998; Freire-de-Lima et al., 2006; Cai et al., 2016). Thus, efferocytosis plays a critical, amplifying role in the resolution response such that it acts as both an effector and a source of resolution mediators.

The role of T cells in resolution is emerging as a critically important topic, and most studies focus on how resolving mediators affect T cell biology. For example, lipoxins and T helper 2 (Th2)-cell-derived protectin D1 suppresses T cell pro-inflammatory cytokines and infiltration into inflammatory sites (Buckley et al., 2014). Conversely, pro-inflammatory leukotriene B₄ (LTB₄) has been shown to dose-dependently decrease the differentiation of naive T cells into regulatory T (Treg) cells, favoring instead the generation of Th17 cells (Chen et al., 2009). The topic of Treg cells is highly relevant because they secrete proteins, such as interleukin-10 (IL-10) and amphiregulin, that promote tissue repair (D'Alessio et al., 2009; Weirather et al., 2014; Arpaia et al., 2015). However, remarkably little is known about how specific resolution processes are affected by Treg cells. In this context, we sought to identify whether Treg cells can promote efferocytosis and, if so, to elucidate key mechanisms. We now show both *in vitro* and *in vivo* that Treg cells can indeed boost the ability of macrophages to carry out efferocytosis during resolution responses. A key mechanistic component involves the induction of IL-10 in macrophages by Treg-cell-derived IL-13. IL-10, via an autocrine-paracrine pathway that affects the guanine nucleotide exchange factor (GEF) Vav1 and the GTPase Rac1, enables macrophages to optimally internalize apoptotic cells. Enhancement of macrophage efferocytosis by Treg cells was evident in three models of inflammation, including

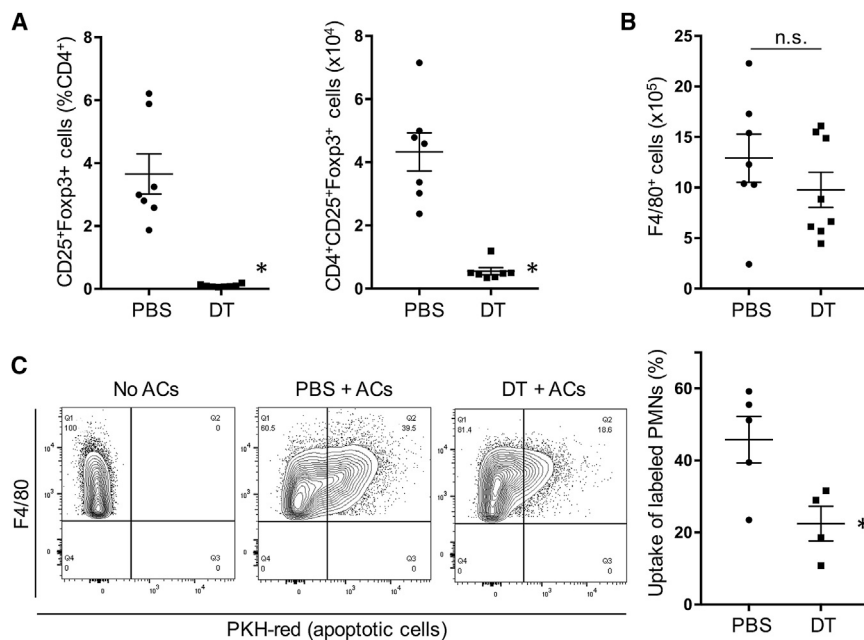


Figure 1. Treg Cell Depletion Following Zymosan-Induced Peritonitis Reduces the Efferocytic Capacity of Peritoneal Macrophages

Foxp3-human DTR mice were injected i.p. with 0.1 mg zymosan at day 0 and then with 50 μ g/kg DT at day 4 and 15 μ g/kg DT at days 6 and 8. The vehicle control for DT was PBS.

(A and B) Peritoneal lavage fluid of one cohort of DT- and PBS-treated mice sacrificed at day 11 was analyzed for Treg cells, either as a percentage of CD4 cells that were CD25⁺ Foxp3⁺ or as an absolute number per mouse, and for the total number of peritoneal F4/80⁺ macrophages ($n = 7$ mice per group; $p < 0.05$, two-tailed Student's *t* test; n.s., non-significant). Data displayed represent one of five independent experiments and are means \pm SEM.

(C) At day 11, another cohort of DT- and PBS-treated mice was injected i.p. with PKH-red-labeled apoptotic cells (ACs), and 45 min later lavage fluid was analyzed by flow cytometry for the percentage of F4/80⁺ macrophages that had incorporated the labeled neutrophils ($n = 4$ or 5 mice per group; $p < 0.05$, two-tailed Student's *t* test). Data displayed represent one of two independent experiments and are means \pm SEM.

atherosclerosis, a critically important disease process characterized by defects in Treg cells, efferocytosis, and resolution. These findings reveal a specific role for Treg cells in inflammation resolution and tissue repair and thereby add to the mechanistic basis for the development of Treg-cell-enhancing therapy for chronic inflammatory diseases.

RESULTS

Treg Cell Depletion Reduces the Efferocytic Capacity of Peritoneal Macrophages during Resolution of Inflammation

To test the hypothesis that Treg cells promote efferocytosis during inflammation resolution, we began with a well-established model of acute inflammation and its resolution, zymosan-induced peritonitis. Low-dose zymosan (0.1 mg) elicits a neutrophil-mediated inflammatory response followed by a decrease in neutrophil numbers and a sharp increase in Treg cells (Newson et al., 2014). We reasoned that this two-phase response might involve Treg-cell-mediated enhancement of efferocytosis of dying neutrophils by macrophages during the resolution phase. Accordingly, we asked whether Treg cell depletion at the onset of resolution would reduce macrophage efferocytic capacity in this model. To accomplish this goal, we depleted Treg cells by injecting diphtheria toxin (DT) into mice expressing the human DT receptor driven by the *Foxp3* promoter (*Foxp3*-hDTR mice) (Saito et al., 2001). DT or PBS was given on days 4, 6, and 8 after zymosan injection. On day 11, when Treg cell numbers typically peak (Newson et al., 2014), we found that peritoneal fluid Treg cells were markedly depleted in DT-treated mice (Figure 1A). In contrast, macrophage numbers were not statistically different between the two groups of mice (Figure 1B). In order to evaluate the efferocytic capacity of peritoneal macrophages *in vivo*, we injected the peritoneum with fluorescently labeled apoptotic

neutrophils. After 45 min, the peritoneal cells were collected by lavage and analyzed by flow cytometry. Uptake of the injected apoptotic neutrophils by peritoneal F4/80⁺ macrophages in Treg-cell-depleted mice was \sim 50% lower than that in PBS-treated control mice (Figure 1C). These data suggest that Treg cells play an important role in the clearance of apoptotic cells during the resolution phase of zymosan-induced peritonitis.

Treg Cell Depletion during the Resolution Phase after Acute Lung Injury Reduces Efferocytosis by Airspace Macrophages

Treg cells are required for timely inflammation resolution in lipopolysaccharide (LPS)-induced acute lung injury (ALI) (D'Alessio et al., 2009). Moreover, murine models and clinical data suggest that efficient efferocytosis following injury is critical for lung repair (Schmidt and Tuder, 2010). In order to determine whether Treg cells promote macrophage efferocytosis during ALI, we subjected *Foxp3*-hDTR mice to LPS-induced ALI. Mice were treated with intranasal LPS on day 0 and then given DT injections (or PBS) on day 1 or days 1, 3, and 5. To first validate the model, we showed that DT treatment on day 1 caused marked depletion of FoxP3⁺ Treg cells by day 4 in both bronchoalveolar lavage (BAL) fluid and in whole lung tissue (Figures 2A and 2B). Of note, Treg cell depletion did not affect the number of resident alveolar (F4/80⁺CD11c^{high}SiglecF⁺) or exudate (F4/80⁺CD11c^{high}SiglecF⁻) macrophages (Figure 2C) and did not lead to any changes in blood leukocyte numbers (Figure S1A). In the experiment in which mice were injected with PBS or DT on days 1, 3, and 5, histopathologic injury scoring (Matute-Bello et al., 2011) by a blinded observer revealed that there was a trend toward improvement in the control mice between days 4 and 7 on the basis of neutrophil numbers in alveolar and interstitial spaces, airway debris, and alveolar septal thickening (Figures S1B and S1C). This improvement was not

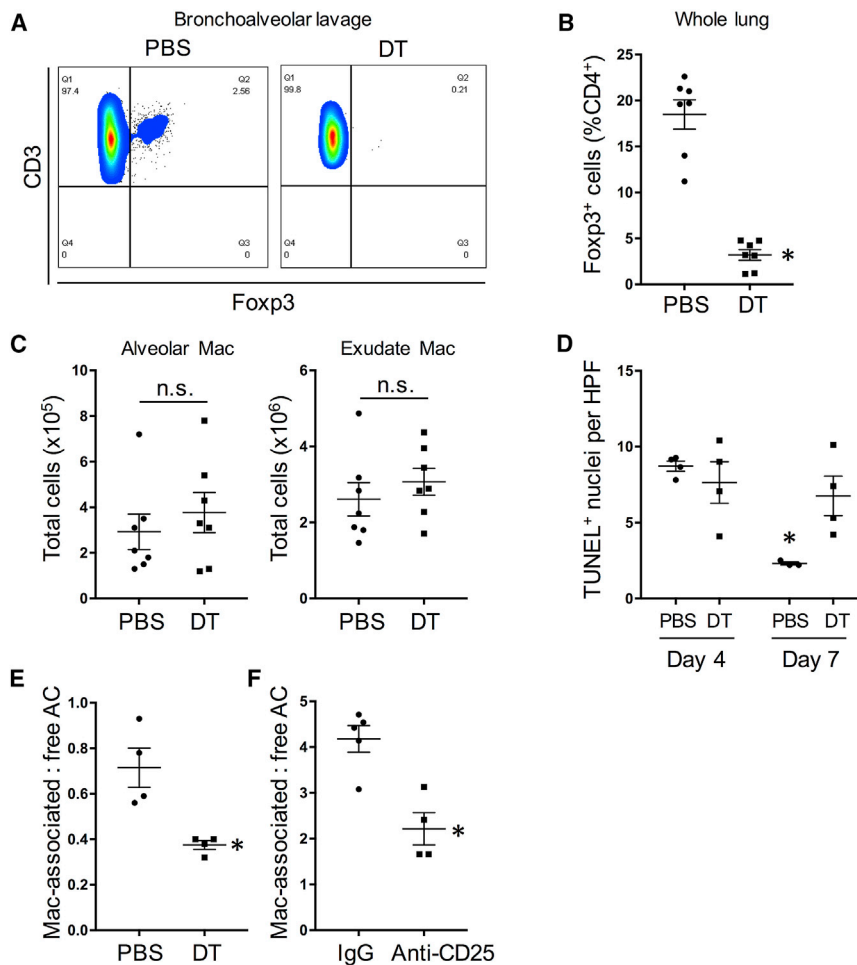


Figure 2. Treg Cell Depletion Decreases Efferocytosis by Macrophages in LPS-Induced ALI

Foxp3-human DTR mice were treated with intranasal LPS on day 0 and then given DT injections (or PBS) on day 1 (A–C and E) or days 1, 3, and 5 (D). (A) Representative flow-cytometry plots of *Foxp3*⁺ Treg cells in the bronchoalveolar lavage fluid of PBS- and DT-treated mice at day 4. Data displayed represent one of three independent experiments.

(B) Quantification of the percentage of *Foxp3*⁺ T cells in whole lung of PBS- and DT-treated mice at day 4 (n = 7 mice per group; *p < 0.05, two-tailed Student's t test). Data represent means ± SEM.

(C) Quantification of alveolar and exudate macrophages (Mac) of PBS- and DT-treated mice at day 4 (n = 7 mice per group; n.s., not significant by two-tailed Student's t test). Data represent means ± SEM.

(D) Quantification of TUNEL⁺ cells in lung sections per high-power field (HPF) of mice at days 4 and 7 (n = 3 or 4 mice per group; *p < 0.05 versus all other groups, two-way ANOVA, Sidak's multiple-comparisons test). Data represent means ± SEM.

(E) Quantification of day 4 lung tissue for TUNEL⁺ apoptotic cells (ACs) that were either associated with *F4/80*⁺ macrophages or not associated with macrophages ("free") (n = 4 mice per group; *p < 0.05, two-tailed Student's t test). Data represent means ± SEM.

(F) The same as in (E), except that Treg cells were depleted in LPS-ALI WT mice with anti-CD25 antibody (with IgG as a control), as described in the STAR Methods; see Figure S2 (n = 4 or 5 mice per group; *p < 0.05, two-tailed Student's t test). Data displayed represent one of two independent experiments and are means ± SEM. Please also see Figure S1.

seen in the Treg-cell-depleted mice, resulting in a significantly worse histological score in these mice than in control mice at day 7.

As a prelude to assaying efferocytosis, we assayed dead cell content in the above day-1-3-5 DT experiment and found that the number of apoptotic cells, assessed by terminal deoxynucleotidyl transferase-mediated dUTP nick end labeling (TUNEL), declined between days 4 and 7 in control mice, consistent with efficient efferocytosis. In contrast, the number of apoptotic cells remained elevated in Treg-cell-depleted mice at day 7 (Figure 2D). To directly examine efferocytosis in day 4 lung tissue, we quantified the ratio of TUNEL⁺ nuclei (dead cells) associated with *Mac-3*⁺ macrophages to dead cells not associated with macrophages ("free") (Thorpe et al., 2008). The data showed that Treg cell depletion significantly reduced efferocytosis (Figures 2E and S1D [top]). A similar result was obtained when Treg cell depletion was accomplished by anti-CD25 antibody treatment of wild-type (WT) mice (Sutmoller et al., 2001), i.e., rather than DT treatment of *Foxp3*-human DTR mice (Figures 2F, S1D [bottom], and S1E). Because acute depletion of Treg cells can activate adaptive immune responses that might impair efferocytosis, we conducted an ALI experiment in *Rag1*^{-/-} mice, which lack mature B and T cells. Compared with efferocytosis in

the lungs of WT mice, efferocytosis was lower in the lungs of *Rag1*^{-/-} mice, which lack Treg cells. These data are consistent with the above results from DT-treated *Foxp3*-hDTR mice. Moreover, partial Treg cell reconstitution in the lungs of *Rag1*^{-/-} mice partially improved efferocytosis by lung macrophages (Figures S1F and S1G). Thus, as with peritonitis, Treg cells promote efferocytosis in ALI, and this process is independent of B cells and effector T cells.

Treg Cell Depletion Disrupts Apoptotic Cell Internalization and *Rac1* Activation in Macrophages

In preparation for mechanistic studies of how Treg cell depletion decreases efferocytosis, we first determined whether we could recapitulate the Treg-cell-depletion-mediated defect in efferocytosis *ex vivo*. To that end, peritoneal macrophages were isolated from PBS- or DT-treated *Foxp3*-hDTR mice 11 days after zymosan and then incubated *ex vivo* with fluorescently labeled apoptotic cells at 37°C. The macrophages from DT-treated mice showed lower efferocytosis than macrophages from control mice (Figure 3A, left). We next conducted this experiment at 4°C, which allows apoptotic cell binding but prevents uptake. Macrophages from control and DT mice showed equal apoptotic cell binding (Figure 3A, right), suggesting that the

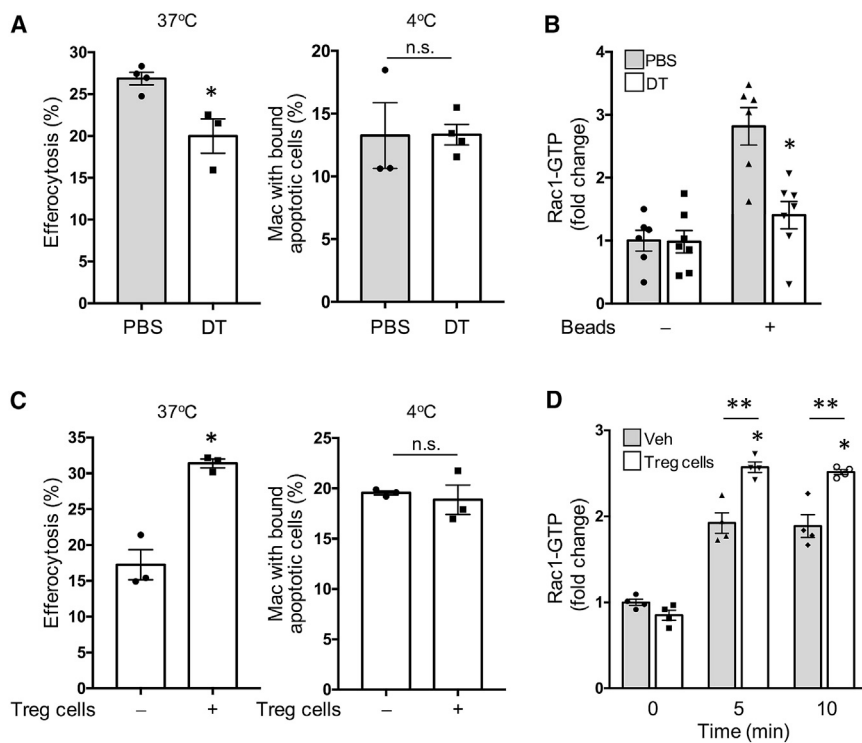


Figure 3. Macrophages from Treg-Cell-Depleted Mice Show Decreased Apoptotic Cell Uptake after Binding and Impaired Rac1 Activation

(A) Macrophages were isolated at day 11 from the peritoneal lavage fluid of zymosan-treated Foxp3-hDTR mice treated with PBS or DT, as in Figure 1. The cells were then incubated with labeled apoptotic cells at 37°C or 4°C (n = 4 mice per group; *p < 0.05, n.s., not significant by two-tailed Student's t test). Data displayed represent one of two independent experiments and are means ± SEM.

(B) A similar set of macrophages was incubated with or without polystyrene beads for 15 min and then assayed for GTP-bound Rac1 (n = 4 mice per group; *p < 0.05 versus all other groups, two-way ANOVA, Sidak's multiple-comparisons test). Data displayed represent one of two independent experiments and are means ± SEM.

(C) Bone-marrow-derived macrophages were incubated with or without splenic Treg cells for 48 hr and then assayed for efferocytosis (37°C) or apoptotic cell binding (4°C) (n = 3 wells; *p < 0.05, n.s., not significant by two-tailed Student's t test). Data displayed represent one of three independent experiments and are means ± SEM.

(D) Same as in (C), except that GTP-bound Rac1 was assayed before or 5 or 10 min after the addition of beads (n = 4 wells; *p < 0.05 versus PBS [time 0] and **p < 0.05 for Treg cell versus Veh, two-way ANOVA, Sidak's multiple-comparisons test). Data displayed represent one of two independent experiments and are means ± SEM.

was assayed before or 5 or 10 min after the addition of beads (n = 4 wells; *p < 0.05 versus PBS [time 0] and **p < 0.05 for Treg cell versus Veh, two-way ANOVA, Sidak's multiple-comparisons test). Data displayed represent one of two independent experiments and are means ± SEM. Please also see Figure S2.

defect in efferocytosis in macrophages from Treg-cell-depleted mice was due to impaired engulfment (not binding) of apoptotic cells.

Apoptotic cell engulfment converges on Rho-family GTPase activation, which induces cytoskeletal rearrangement. In particular, Rac1 has been shown to be critical for apoptotic cell engulfment as well as for the internalization of other phagocytic cargo (Ravichandran and Lorenz, 2007). Rac1-GTP increases early after apoptotic cell recognition by membrane receptors, and active Rac1 is recruited to the phagocytic cup, where it promotes F-actin assembly. Thus, we questioned whether macrophages from Treg-cell-depleted mice might have decreased GTP-bound Rac1, a measure of Rac1 activity, during phagocytosis. In pilot experiments, we found a high degree of variability in the assay of Rac1 activity in macrophages incubated with apoptotic cells, perhaps as a result of the effect of proteins in the apoptotic cells themselves. We reasoned that using inert beads as the phagocytic substrate might minimize this problem. We first determined whether macrophages from DT-treated mice had a defect in the uptake of polystyrene beads *ex vivo*, which indeed was the case (Figure S2A). Using this model, we compared Rac1 activation in macrophages from control and DT mice. Whereas GTP-bound Rac1 was significantly increased 20 min after the addition of beads in control macrophages, the bead-induced increase in Rac1 activation was completely abrogated in macrophages from Treg-cell-depleted DT mice (Figure 3B). Thus, preventing macrophages from being exposed to Treg cells during resolution impairs efferocytosis and phagocytosis-associated Rac1 activation.

We next asked whether a Treg-cell-macrophage co-culture model could recapitulate some of these findings. For this purpose, bone-marrow-derived macrophages were incubated for 48 hr with or without splenic Treg cells (Figure S2B) and then assayed for the uptake of fluorescently labeled apoptotic Jurkat cells and for bead-induced Rac1 activation. Consistent with the previous data, Treg cells enhanced apoptotic cell uptake without altering binding and increased bead-induced Rac1 activation (Figures 3C and 3D). We also investigated whether Treg-cell-macrophage co-culture would induce other macrophage changes suggestive of a more pro-resolving phenotype. Indeed, Treg cells led to an upregulation in macrophages of mRNAs for genes associated with resolution, including *Arg1*, *Retnla* (Fizz1), and *Mrc1* (CD206) (Figure S2C). We also compared mRNA from peritoneal macrophages obtained from mice at day 8 after zymosan injection, which is prior to the influx of Treg cells, with macrophages at day 10, which is the time when Treg cell influx into the peritoneum reaches its peak. Day 10 macrophages showed decreased expression of the pro-inflammatory genes *Il1b* and *Il6* and increased expression of the pro-resolving gene *Mrc1* (CD206), and there were trends toward decreased *Tnfa* and increased *Arg1* (Figure S2D). In summary, Treg cells can directly enhance the ability of macrophages to internalize apoptotic cells or a non-cellular phagocytic substrate, and this action of Treg cells is associated with activation of Rac1. In line with the role of efferocytosis in resolution, Treg cells might also shift the phenotype of macrophages toward a more general pro-resolving functional state.

Enhancement of Efferocytosis by Treg Cells Involves Treg-Cell-Induced Macrophage IL-10 Production

A number of secreted molecules, including IL-10, have been described to be important for Treg cell function (Arpaia et al., 2015). Because IL-10 enhances efferocytosis by macrophages (Ogden et al., 2005; Michlewska et al., 2009; Michalski et al., 2016), we investigated whether it is required for Treg-cell-mediated enhancement of macrophage efferocytosis. Using the zymosan peritonitis model, we first compared the efferocytic capacity of peritoneal macrophages from *I110*^{-/-} and WT mice *in vivo*. On day 11 after zymosan injection, WT and *I110*^{-/-} mice were injected intraperitoneally (i.p.) with fluorescently labeled apoptotic neutrophils, and after 45 min, uptake of the labeled cells by exudate macrophages was evaluated by flow cytometry. We found that apoptotic cell uptake was lower in *I110*^{-/-} mice than in WT mice (Figure 4A). Of note, there was no difference in the percentage of peritoneal Treg cells (CD4⁺CD25⁺) between WT and *I110*^{-/-} mice (Figure S3A). As further validation, a neutralizing anti-IL-10 antibody injected i.p. 48 hr before the harvest of peritoneal macrophages also caused a reduction in *ex vivo* efferocytosis (Figure 4B).

To determine whether Treg cells are the source of efferocytosis-enhancing IL-10, we injected WT or *I110*^{-/-} splenic Treg cells into the peritoneum of naive WT mice. After 3 days, macrophages harvested from the peritoneal exudates of these mice were assayed for uptake of labeled apoptotic cells. We found that that injection with WT and *I110*^{-/-} Treg cells enhanced subsequent *ex vivo* efferocytosis similarly (Figure 4C), suggesting that IL-10 production by Treg cells is dispensable for this process. We next tested whether expression of IL-10 by macrophages is required for the ability of Treg cells to enhance efferocytosis. For this purpose, WT and *I110*^{-/-} bone-marrow-derived macrophages were cultured with WT splenic Treg cells and then assayed for efferocytosis *in vitro*. Whereas Treg cells enhanced efferocytosis in WT macrophages as expected, they did not have this effect on *I110*^{-/-} macrophages (Figure 4D) or on macrophages from mice lacking the β subunit of the IL10 receptor (*I110rb*^{-/-}), which is required for IL-10 signaling (Spencer et al., 1998; Figure S3B). Similar results were found when the endpoint of this assay was bead-mediated Rac1 activation (Figure 4E). Thus, Treg-cell-mediated enhancement of efferocytosis requires macrophages to express both IL-10 and the IL-10 receptor, suggesting an autocrine-paracrine pathway in which Treg-cell-stimulated macrophage IL-10 production enhances apoptotic cell internalization by IL-10-mediated Rac1 activation in macrophages.

To provide further support for this hypothesis, we showed that incubation of cultured macrophages with Treg cells markedly increased the expression of *I110* mRNA in the macrophages and the expression of the macrophage IL-10 target gene *Bcl3* in WT but not *I110*^{-/-} macrophages (Figure 4F). Consistent with the findings above, Treg-cell-induced *I110* and *Bcl3* in macrophages did not depend on IL-10 expression by the Treg cells (Figures S3C and S3D). Finally, incubation of macrophages with recombinant IL-10 enhanced efferocytosis without increasing apoptotic cell binding (Figures 4H and S3E) and increased Rac1 activation (Figure 4H). IL-10 also enhanced efferocytosis in human macrophages (Figure S3F). These combined data support a mechanism in which Treg

cells send a transcellular signal that induces *I110* in macrophages and then IL-10 acts in an autocrine-paracrine manner in macrophages to enhance Rac1-mediated apoptotic cell internalization.

The Treg-Cell-IL-10-Efferocytosis Pathway Is Functional in a Complex Inflammatory Disease Model

In atherosclerosis, the disease process underlying the leading causes of death in the industrialized world, defective efferocytosis and decreased Treg cells drive disease progression, but these two processes have not been previously linked (Schrijvers et al., 2005; Yurdagul et al., 2018; Ait-Oufella et al., 2006). In this context, we focused on the specific question as to whether expansion of Treg cells during advanced atherosclerosis progression can promote lesional efferocytosis in an IL-10-dependent manner. 12-week-old Western-diet (WD)-fed *Ldlr*^{-/-} mice, which develop aortic root atherosclerotic lesions with defective efferocytosis (Thorp et al., 2008), were treated with IL-2 complex (IL-2C) consisting of recombinant IL-2 and anti-IL-2 monoclonal antibody to expand Treg cells (Boyman et al., 2006; Dinh et al., 2012; Foks et al., 2011). The complex was administered for 3 consecutive days and then once every 5 days thereafter for a 3-week period, during which time the WD was continued. Some of the mice were also treated twice weekly during this 3-week period with an anti-IL-10 neutralizing antibody, and the rest of the mice received control IgG antibody. 5 days after the initiation of IL-2C treatment, there was >5-fold elevation of circulating Treg cells, and this was unaffected by anti-IL-10 co-administration (Figure 5A). At the time of sacrifice, Treg cells were also significantly higher in the spleens of IL-2C-treated mice (Figure 5B). We also measured phospho-STAT3 in splenocytes by flow cytometry as a measure of IL-10 bioactivity and found that this endpoint was significantly increased by IL-2C but not by the combination of IL-2C and anti-IL-10 (Figure 5C).

Treg cell expansion with or without IL-10 neutralization had no effect on body weight, plasma cholesterol, plasma triglycerides, or fasting glucose (Figures S4A–S4D). Moreover, as expected for this short treatment period, there were no differences in lesional area or macrophage content among the four groups (Figures S4E and S4F). However, as predicted by the hypothesis, IL-2C treatment significantly improved the ratio of macrophage-associated to macrophage-free apoptotic cells, indicating enhanced efferocytosis, and this improvement was abrogated by IL-10 neutralization (Figure 5D). The improvement in efferocytosis in the IL-2C group (second group) and the prevention of this effect in the anti-IL-10 group (third group) could not be explained by changes in cell death because the total number of TUNEL⁺ lesional cells was similar among these two groups and the Veh-IgG control group (first group) (Figure S4G). Although the number of apoptotic cells was modestly higher in the lesions of mice treated with anti-IL-10 alone (fourth group), the data in Figure 5D show that lesional efferocytosis was similar between this group and the control group (representative images are shown in Figure S4H). These data support the conclusion that Treg cell expansion can enhance efferocytosis in an IL-10-dependent manner in a critically important disease model that encompasses both decreased Treg cells and defective efferocytosis.

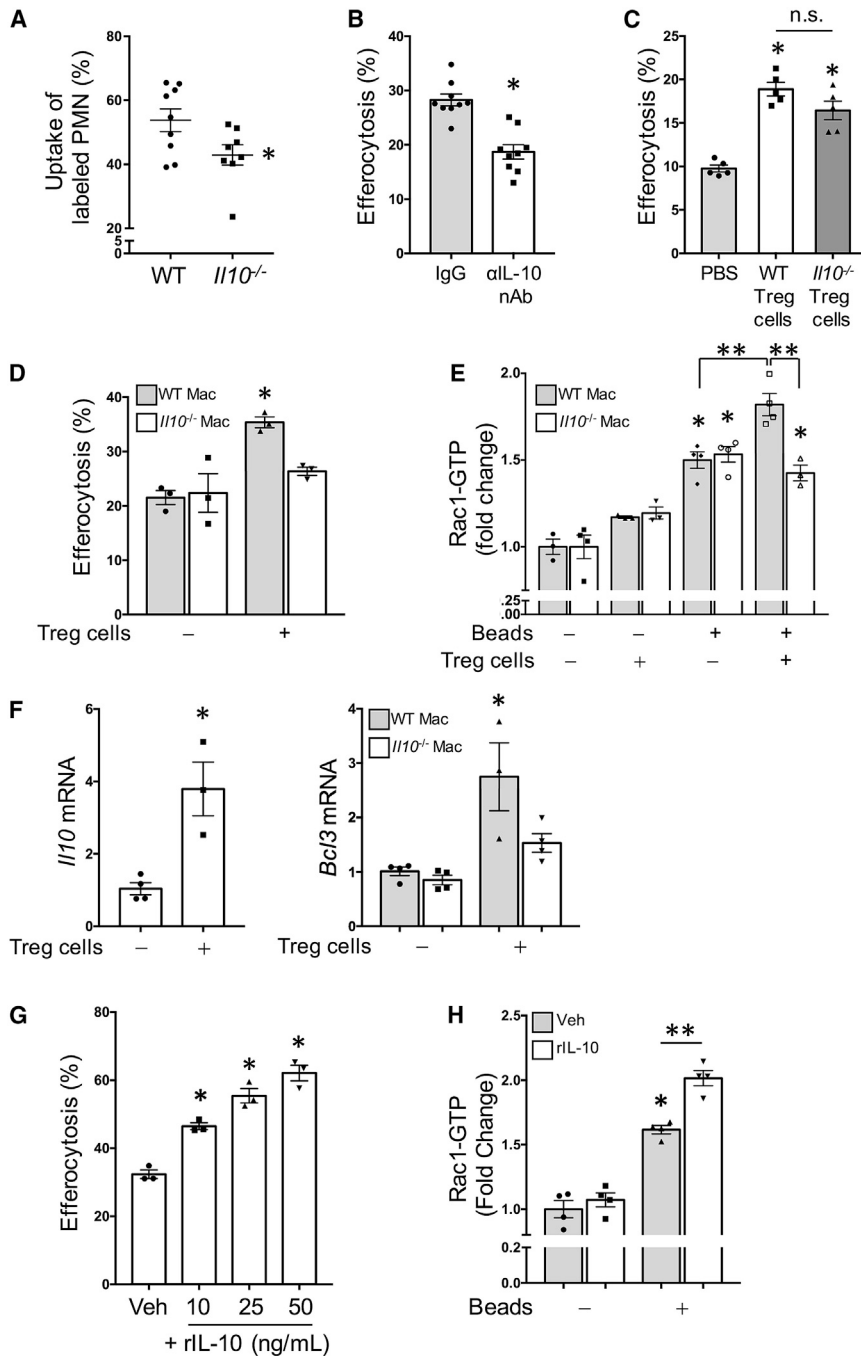


Figure 4. Treg-Cell-Mediated Enhancement of Efferocytosis Requires Macrophage IL-10 Expression

(A) Efferocytosis of i.p. injected labeled neutrophils was assayed at day 11 in zymosan-treated WT or *Il10*^{-/-} mice as in Figure 1C (n = 9 or 10 mice per group; *p < 0.05, two-tailed Student's t test). Data represent means ± SEM.

(B) WT mice were injected i.p. with neutralizing antibody to IL-10 or control IgG, and 48 hr later, peritoneal macrophages were harvested and then assayed for efferocytosis *ex vivo* (n = 3 wells per condition; *p < 0.05, two-tailed Student's t test). Data represent means ± SEM.

(C) WT mice were injected i.p. with Treg cells from WT or *Il10*^{-/-} mice or vehicle control (PBS). Peritoneal macrophages were harvested and then assayed for efferocytosis *ex vivo* (n = 5 mice per group; *p < 0.05 versus PBS; n.s., non-significant, one-way ANOVA, Tukey's post hoc analysis). Data displayed represent one of two independent experiments and are means ± SEM.

(D) Bone-marrow-derived macrophages from WT or *Il10*^{-/-} mice were incubated with or without splenic Treg cells from WT mice and then assayed for efferocytosis *in vitro* as in Figure 3C (n = 3 wells; *p < 0.05 versus all other groups, two-way ANOVA, Sidak's multiple-comparisons test). Data represent means ± SEM.

(E) Bead-induced GTP-bound Rac1 was assayed in WT or *Il10*^{-/-} macrophages incubated with or without Treg cells as in Figure 3D (n = 4 wells; *p < 0.05 versus no beads and **p < 0.05 for the indicated pairings, two-way ANOVA, Sidak's multiple-comparisons test). Data displayed represent one of two independent experiments and are means ± SEM.

(F) WT or *Il10*^{-/-} bone-marrow-derived macrophages were incubated with or without Treg cells and then assayed for *Il10* mRNA (n = 3 or 4 wells; *p < 0.05, two-tailed Student's t test) or *Bcl3* mRNA (n = 3 or 4 wells; *p < 0.05 versus all other groups, two-way ANOVA, Sidak's multiple-comparisons test). Data represent means ± SEM.

(G) Bone-marrow-derived macrophages were pre-treated for 48 hr with the indicated concentrations of rIL-10 and then assayed for efferocytosis (n = 3 wells; *p < 0.05 versus Veh, one-way ANOVA, Tukey's post hoc analysis). Data represent means ± SEM.

(H) Bone-marrow-derived macrophages were pre-treated for 48 hr with 10 ng/mL rIL-10 and then assayed for GTP-bound Rac1 10 min after

exposure to beads as in Figure 4D (n = 3 wells; *p < 0.001 versus no beads and **p < 0.001 for rIL-10 versus Veh, two-way ANOVA, Sidak's multiple-comparisons test). Data displayed represent one of two independent experiments and are means ± SEM.

Please also see Figure S3.

Treg-Cell-Derived IL-13 Stimulates IL-10 Production and Efferocytosis by Macrophages

To determine how Treg cells might stimulate macrophages to produce IL-10, we considered a number of Treg-cell-derived secretory molecules and focused on IL-13 as a candidate (Ochoa-Repáraz et al., 2008; Kambayashi et al., 1996; Hutchins et al., 2012). We first showed that stimulation of IL-2-treated

CD25⁺ Treg cells with CD3 and CD28 increased both *Il13* mRNA (Figure S5A) and secreted IL-13 (Figure 6A). Next, incubation of macrophages with recombinant IL-13 induced *Il10* and enhanced efferocytosis in an IL-10-receptor-dependent manner (Figures 6B and 6C). Most importantly, unlike WT Treg cells, Treg cells from *Il13*^{-/-} mice did not significantly increase efferocytosis above that seen with no Treg cells (Figure 6D, left). Similar

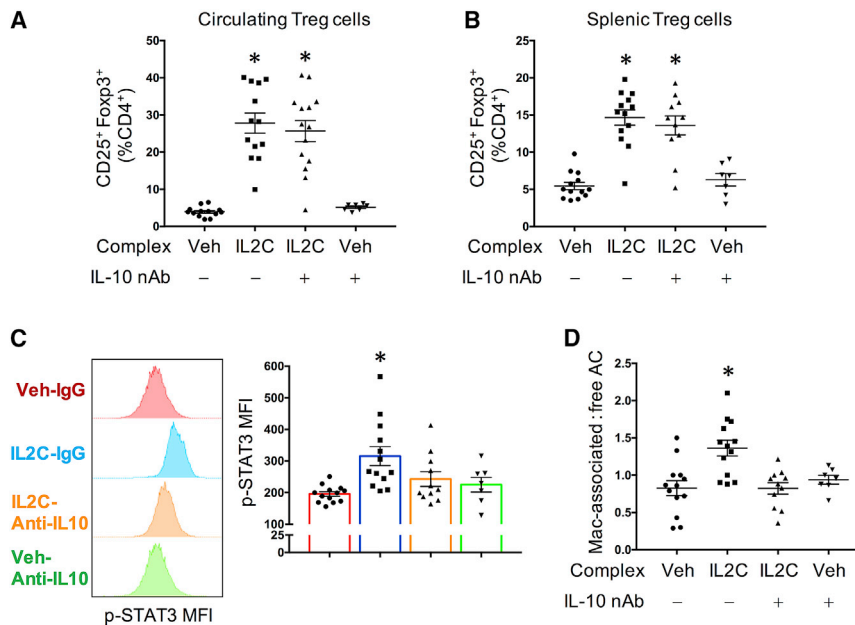


Figure 5. Treg Cell Expansion Improves Lesional Efferocytosis in WD-Fed *Ldlr*^{-/-} Mice in an IL10-Dependent Manner

Ldlr^{-/-} mice were fed a WD for 12 weeks and then treated with a complex of recombinant IL-2 and anti-IL2 (IL2C) or vehicle control for 3 consecutive days and then once every 5 days thereafter for a 3-week period, during which time the mice were continued on a WD. The mice were also treated twice weekly with an IL-10-neutralizing antibody (nAb) or an IgG control antibody during this 3-week period.

(A and B) Circulating Treg cells 5 days after initiation of the treatment and splenic Treg cells 3 weeks after antibody treatment in the four groups of mice (n = 7–13 mice per group; *p < 0.05 versus groups without IL-2C, one-way ANOVA, Sidak’s multiple-comparisons test). Data represent means ± SEM.

(C) Splenocytes from the four groups of mice were assayed for phospho-STAT3 by flow cytometry and quantified as mean fluorescence intensity (MFI) (n = 7–13 mice per group; *p < 0.05 versus all other groups, one-way ANOVA, Sidak’s multiple-comparisons test). Data represent means ± SEM.

(D) Aortic root lesions of the four groups of mice

were assayed for *in situ* efferocytosis by quantification of the ratio of apoptotic cells (ACs) that were associated with lesional macrophages or not (free) (n = 7–13 mice per group; *p < 0.05 versus all other groups, one-way ANOVA, Sidak’s multiple-comparisons test). Data represent means ± SEM.

Please also see Figure S4.

findings were obtained when a Transwell system was used to separate the macrophages and Treg cells, indicating that Treg-cell-macrophage contact was not needed for Treg-cell-induced efferocytosis in macrophages (Figure 6D, right) or when an anti-IL-13 neutralizing antibody was used instead of *Il13*^{-/-} Treg cells (Figure S5B). However, when IL-13 was silenced in macrophages, WT Treg cells still enhanced macrophage IL-10 expression (Figure S5C), indicating that Treg-cell-derived IL-13 rather than macrophage-derived IL-13 is important in this pathway. Finally, we examined the effect of WT and *Il13*^{-/-} Treg cells on the uptake of polystyrene beads, live cells, and heat-induced necrotic cells. As with apoptotic cells, Treg cells increased the uptake of polystyrene beads in an IL-13-dependent manner (Figure S5D, left graph), which is consistent with the finding that Treg cells stimulate efferocytosis via Rac1-mediated internalization. As expected, there was no detectable uptake of live cells by macrophages, and this did not change when Treg cells were added. Necrotic cell uptake by macrophages was substantial even without co-culture with Treg cells and was not further enhanced by Treg cells (Figure S5D, right graph).

To assess the role of IL-13 *in vivo*, we turned to the peritoneal adoptive-transfer model described in Figure 4B and found that enhancement of efferocytosis by i.p. injected Treg cells was abrogated when the mice were co-injected with anti-IL-13 neutralizing antibody at the time of Treg cell injection (Figure 6E). In addition, we utilized the *Foxp3*-hDTR mouse model and showed that whereas WT Treg cells were able to rescue deficient efferocytosis in Treg-cell-depleted mice, delivery of an equal number of *Il13*^{-/-} Treg cells failed to do so (Figures 6F and S5E). We then tested this pathway in a disease model by utilizing the LPS-induced model of acute lung injury in *Foxp3*-hDTR mice

described in Figure 2. As expected, DT treatment caused a loss of Treg cells in both the lungs and spleen (Figure S5F, groups 1 and 2), and consistent with our previous experiment, the lungs of mice depleted of Treg cells had lower efferocytosis than those of control mice (Figure 6G, groups 1 and 2). We then tested the effect of partially restoring the lungs of DT-treated mice with WT versus *Il13*^{-/-} Treg cells by using the strategy described for the *Rag1*^{-/-} experiment in Figures S1F and S1G. Similar to that experiment, administering WT and *Il13*^{-/-} Treg cells by the intranasal route was able to partially restore Treg cells in the lungs of DT-treated mice without any increase in Treg cells in the spleens (Figure S5F, groups 3 and 4). Most importantly, whereas the lungs of mice treated with WT Treg cells showed partial restoration of efferocytosis, the lungs of mice treated with *Il13*^{-/-} Treg cells showed less improvement in efferocytosis (Figure 6G, groups 3 and 4).

We next questioned whether different types of macrophages might respond differently to Treg cell stimulation. It has been reported previously that resident macrophages have higher rates of efferocytosis than do recruited macrophages (Newson et al., 2014). Accordingly, we isolated resident peritoneal macrophages from naive mice (day 0 macrophages) and from mice that had received 0.1 mg of zymosan (a source of predominantly recruited macrophages) 8 days previously. These macrophages were co-cultured *ex vivo* with either WT or *Il13*^{-/-} Treg cells for 48 hr and then assayed for efferocytosis. As predicted, day 0 macrophages were better efferocytosis under basal conditions. Most importantly, whereas both day 0 and day 8 macrophages showed enhanced efferocytosis in response to WT Treg cells, the day 0 macrophages demonstrated a 20.1% increase, and the day 8 macrophages demonstrated a 66.4% increase (Figure S6A, groups 1 and 2 and groups 4 and 5). In contrast,

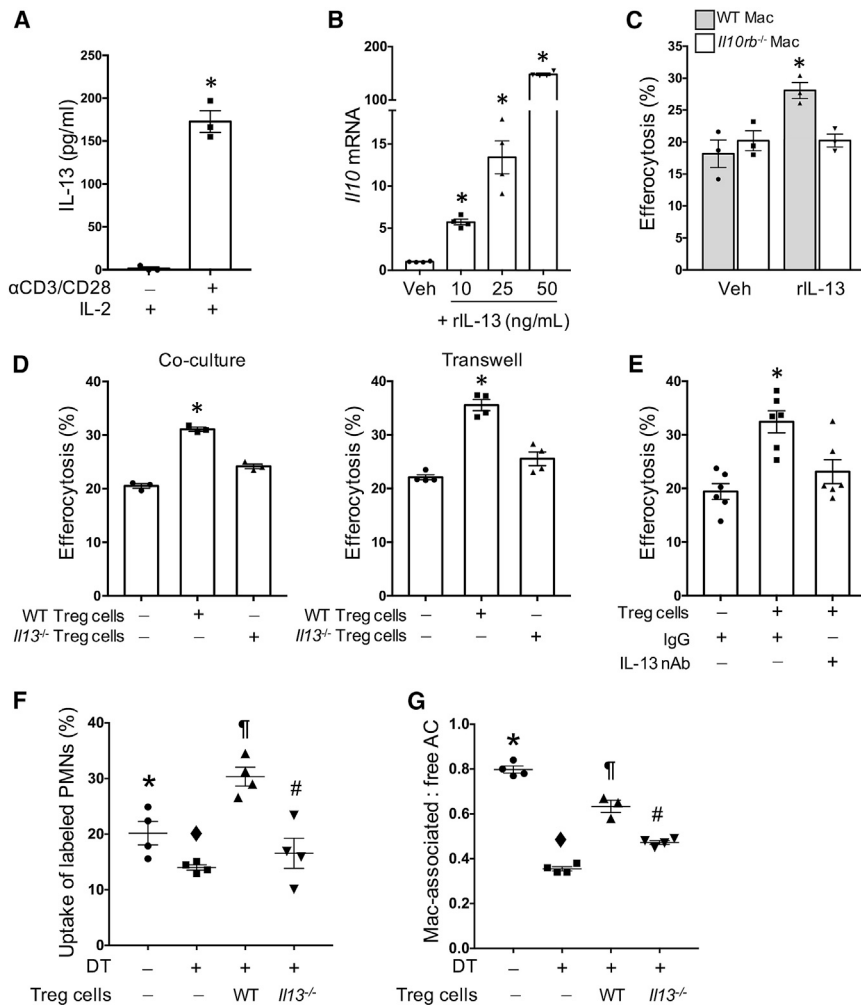


Figure 6. Treg-Cell-Derived IL-13 Stimulates Macrophage Efferocytosis in an IL-10-Dependent Manner

(A) Treg cells were isolated from the spleens of WT mice and incubated with the indicated stimuli overnight. Concentrated cell supernatants were assayed for IL-13 by ELISA (n = 3 wells; *p < 0.001, two-tailed Student's t test). Data displayed represent one of three independent experiments and are means ± SEM.

(B) Bone-marrow-derived macrophages were incubated with the indicated concentrations of rIL-13 for 2 hr and then assayed for *I/10* mRNA (n = 4 wells; *p < 0.05 versus Veh, one-way ANOVA, Sidak's multiple-comparisons test). Data represent means ± SEM.

(C) Bone-marrow-derived macrophages from WT or *I/10rb*^{-/-} mice were incubated for 2 days with 10 ng/mL rIL-13 or vehicle control and then assayed for efferocytosis (n = 3 wells; *p < 0.05 versus WT/Veh, two-way ANOVA, Sidak's multiple-comparisons test). Data represent means ± SEM.

(D) Left: macrophages were co-cultured with either WT or *I/13*^{-/-} Treg cells and then assayed for efferocytosis. Right: macrophages were plated on the upper chamber inserts of a 24-well Transwell dish with media, WT Treg cells, or *I/13*^{-/-} Treg cells in the bottom chambers. After 48 hr, the upper chamber inserts (macrophages) were transferred to a well containing fresh media, and efferocytosis was assayed (n = 3 or 4 wells per group; *p < 0.05 versus the other groups, one-way ANOVA, Sidak's multiple-comparisons test). Data displayed represent one of two independent experiments and are means ± SEM.

(E) Mice were injected i.p. with or without Treg cells and with anti-IL-13 or control IgG as indicated. Peritoneal macrophages from these mice were then assayed for efferocytosis *ex vivo* (n = 6 wells; *p < 0.05 versus the other groups, one-way ANOVA, Sidak's multiple-comparisons test). Data represent means ± SEM.

(F) Naive *Foxp3*-human DTR mice were injected with PBS or 50 μg/kg DT at day 0 and then 15 μg/kg DT on the morning of day 1. On the afternoon of day 1, 5 × 10⁵ splenic Treg cells from WT or *I/13*^{-/-} mice (or PBS control) were isolated and delivered i.p. to the mice as indicated. After 48 hr, mice were injected i.p. with PKH-red-labeled apoptotic neutrophils (n = 4 mice per group; groups with different symbols are statistically different from each other with a p value ≤ 0.05 by two-way ANOVA, Sidak's multiple-comparisons test). Data represent means ± SEM.

(G) *Foxp3*-human DTR mice were treated with intranasal LPS on day 0 and then given DT injections (or PBS) on day 1. 2 × 10⁶ WT or *I/13*^{-/-} Treg cells (or PBS) were delivered intranasally to mice on the afternoon of day 1. TUNEL⁺ apoptotic cells (AC) that were either associated with Mac-3⁺ macrophages or not associated with macrophages (free) were quantified (n = 3 or 4 mice per group; groups with different symbols are statistically different from each other with a p value ≤ 0.05 by two-way ANOVA, Sidak's multiple-comparisons test). Data represent means ± SEM.

Please also see Figures S5 and S6.

I/13^{-/-} Treg cells failed to boost efferocytosis in either day 0 or day 8 macrophages (Figure S6A, groups 3 and 6).

Given the role for both Treg cell IL-13 and macrophage IL-10, we sought to determine whether these are dynamically regulated in the peritonitis model. Day 4 and 10 post-zymosan-injection mice were examined, during which time Treg cells showed a marked increase and macrophages showed a slight decrease (Figure S6B). As predicted by the proposed pathway, IL-13 in the peritoneal exudate rose between days 4 and 10 (Figure S6C). Note that the expression of *I/13* by Treg cells did not rise (Figure S6D), consistent with the idea that the increased number of Treg cells in the peritoneum at day 10 rather than the increased production per cell is responsible for the

observed increase in peritoneal IL-13. Three other predictions were borne out by the data: (1) the concentration of peritoneal IL-10 rose between days 4 and 10 (Figure S6E), (2) this rise coincided with an increase in *I/10* expression by macrophages (Figure S6F), and (3) the expression of *I/13* in macrophages and *I/10* in Treg cells did not change over time (Figures S6G and S6H).

In summary, the combined *in vitro* and *in vivo* data support a pathway in which activated Treg cells secrete IL-13, which then increases efferocytosis by stimulating macrophages, particularly recruited macrophages, to secrete the efferocytosis-enhancing autocrine-paracrine cytokine IL-10. The finding that *I/13*^{-/-} Treg cells had some ability, albeit minimal, to boost

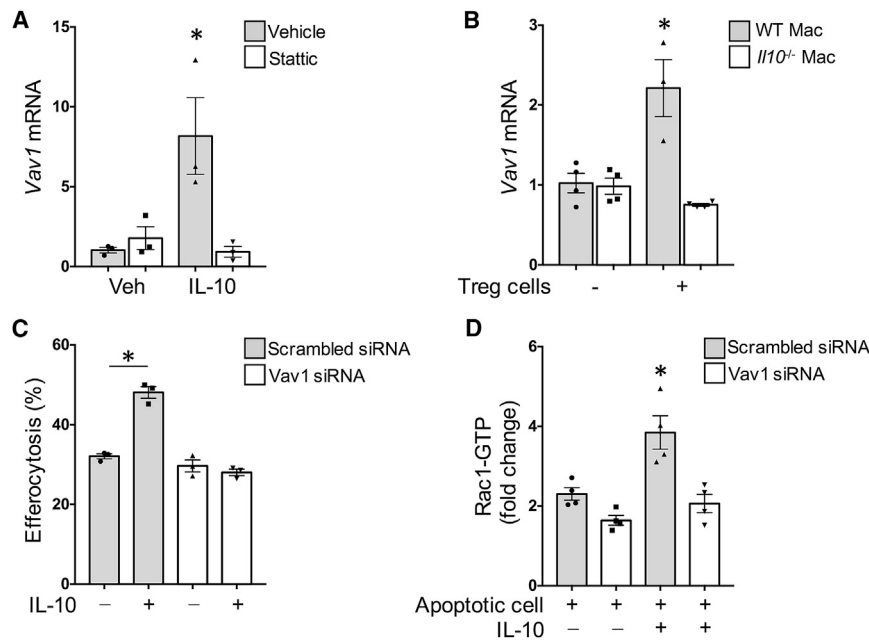


Figure 7. IL-10 and Treg Cells Induce the Rac1 GEF Vav1 in Macrophages, which Is Necessary for the Enhancement of Rac1 Activation and Efferocytosis

(A) Bone-marrow-derived macrophages were incubated with rIL-10 or vehicle control in the absence or presence of the STAT3 inhibitor 6-nitro-benzo[b]thiophene-1,1-dioxide (“Stattic,” 6 μ M) (n = 3 wells; *p < 0.05 versus all other groups, two-way ANOVA, Sidak’s multiple-comparisons test). Data represent means \pm SEM.

(B) WT or *Il10*^{-/-} macrophages were incubated with or without Treg cells and then assayed for Vav1 mRNA (n = 3 or 4 wells; *p < 0.05 versus all other groups, two-way ANOVA, Sidak’s multiple-comparisons test). Data represent means \pm SEM.

(C) Macrophages treated with Vav1 or scrambled siRNA were incubated with or without IL-10 and then assayed for efferocytosis (n = 3 wells; *p < 0.05, two-way ANOVA, Sidak’s multiple-comparisons test). Data displayed represent one of two independent experiments and are means \pm SEM.

(D) Macrophages treated with Vav1 or scrambled siRNA were incubated with or without apoptotic

cells and/or IL-10 and then assayed for GTP-bound Rac1 (n = 4 wells; *p < 0.05 versus all other groups, one-way ANOVA, Sidak’s multiple-comparisons test). Data displayed represent one of two independent experiments and are means \pm SEM.

Please also see [Figure S7](#).

efferocytosis in the DT lung model suggests that Treg cells have an additional pro-efferocytic mechanism in this setting.

IL-10 Signaling Enhances Apoptotic Cell Uptake via Induction of Vav1

As a Rho family GTPase, Rac1 cycles between an active GTP-bound form and an inactive GDP-bound form through the action of GEFs. In considering how IL-10 enhances Rac1 activity to enhance efferocytosis ([Figure 3](#)), we focused on the Rac1 GEF Vav1. Vav1 has been implicated previously in efferocytosis and is a target of STAT3, which is one of the mediators of IL-10 transcriptional programming ([Mondal et al., 2011](#); [Hutchins et al., 2012](#)). We found that IL-10 increased Vav1 expression in macrophages and that this increase was blocked by the STAT3 inhibitor Stattic ([Schust et al., 2006](#)) ([Figures 7A and S7A](#)). Vav1 expression was also induced by Treg cells, and this effect was dependent on IL-10 expression by the macrophages ([Figure 7B](#)). To determine the importance of Vav1 in IL-10-enhanced efferocytosis, we used small interfering RNA (siRNA) to silence Vav1 in macrophages ([Figure S7B](#)) and then tested the effect of IL-10 on efferocytosis and Rac1 activation. Vav1 silencing completely abrogated the enhancement of both efferocytosis and Rac1 activation by IL-10 ([Figures 7C and 7D](#)). Together, the data in [Figures 3, 4, 5, 6, and 7](#) support a mechanism in which Treg cells enhance macrophage efferocytosis through a transcellular signaling pathway in which Treg-cell-derived IL-13 activates an IL-10-Vav1-Rac1 apoptotic cell internalization pathway in macrophages ([Figure S7C](#)).

DISCUSSION

Treg cells, by suppressing the inflammatory activity of both innate and adaptive immune cells and by secreting proteins

involved in tissue repair, are poised to play an important role in the inflammation resolution response ([Gagliani et al., 2015](#); [Newson et al., 2014](#); [D’Alessio et al., 2009](#); [Weirather et al., 2014](#); [Arpaia et al., 2015](#)). Our findings showing that Treg cells boost efferocytosis by macrophages, which is a critically important effector arm of inflammation resolution, fits this idea well. Treg cells carry out this function by using IL-13 as a transcellular mediator: Treg-cell-derived IL-13 stimulates macrophages to produce IL-10, which then acts in an autocrine-paracrine manner to enhance apoptotic cell engulfment via a Vav1-Rac1-mediated mechanism. IL-13 is typically considered to be pro-inflammatory, but it has also been reported to stimulate IL-10 production and inflammation resolution in a murine model of chronic colitis ([Fichtner-Feigl et al., 2014](#)) and to be protective in experimental autoimmune encephalomyelitis ([Ochoa-Repáraz et al., 2008](#)). Although IL-13 appears to be the dominant mechanism *in vitro* and in zymosan-induced peritonitis, it is possible that Treg-cell-mediated enhancement of efferocytosis in other settings might involve additional mechanisms, as suggested by our finding that adoptive transfer of *Il13*^{-/-} Treg cells into the lungs of Treg-cell-depleted mice led to higher lung macrophage efferocytosis than vehicle alone. Thus, it is possible that Treg cells in this model might secrete a protein, in addition to IL-13, that increases macrophage IL-10 ([Chung et al., 2007](#)) or that enhances macrophage efferocytosis by an IL-10-independent mechanism.

Although the Treg-cell-efferocytosis pathway revealed here has not been previously elucidated, the IL-10 component of this pathway integrates well with the results of previous studies ([Ogden et al., 2005](#); [Michlewska et al., 2009](#); [Michalski et al., 2016](#)). One of these studies suggests a mechanistic link to STAT3 activation ([Michalski et al., 2016](#)), which fits well with

the STAT3-Vav1-Rac1 pathway reported here. Another paper reported that Treg cell depletion during ALI is associated with an increase in protein and neutrophils in bronchoalveolar lavage fluid and a worsening of lung histology (Aggarwal et al., 2014), but efferocytosis was not examined. Finally, in considering the findings here, it is interesting to consider how the ability of Treg cells to induce macrophage IL-10 might have a broader role in macrophage-mediated inflammation resolution. For example, a recent report shows that IL-10 can re-program macrophage metabolism in a way that promotes anti-inflammatory and resolution functions (Ip et al., 2017).

The application of our findings to atherosclerosis has particularly important implications. Defective resolution in general and defective efferocytosis in particular play key roles in the progression of relatively benign atherosclerotic lesions into clinically important necrotic plaques (Serhan et al., 2014; Schrijvers et al., 2005; Yurdagul et al., 2018). Moreover, animal and human studies suggest that Treg cells, IL-10, and IL-13 can protect against advanced plaque progression (Schrijvers et al., 2005; Yurdagul et al., 2018; Ait-Oufella et al., 2006; Pinderski et al., 2002; Potteaux et al., 2004; Liu et al., 2006; George et al., 2012; Tziakas et al., 2007; Cardilo-Reis et al., 2012). Our current data now suggest a plausible link among defects in Treg cells, IL-10, IL-13, and efferocytosis in plaque progression and thereby raise the possibility that therapeutically boosting this axis might prevent atherothrombotic disease in subjects at high risk. Likewise, on the basis of the other two *in vivo* models used in this study, this therapeutic strategy could help prevent the pathophysiological consequences of sepsis and inflammatory lung disease, which, like advanced atherosclerosis, are often associated with impaired resolution (Buckley et al., 2014).

STAR★METHODS

Detailed methods are provided in the online version of this paper and include the following:

- KEY RESOURCES TABLE
- CONTACT FOR REAGENT AND RESOURCE SHARING
- EXPERIMENTAL MODEL AND SUBJECT DETAILS
 - Cell Lines
 - Primary Cell Cultures
 - Experimental Animals
- METHOD DETAILS
 - Zymosan-Induced Peritonitis
 - Peritoneal Uptake of Labeled Apoptotic Cells (ACs)
 - Acute Lung Injury
 - Lung Histology
 - *In Situ* Efferocytosis Analysis
 - Flow Cytometry
 - Regulatory T Cell Isolation
 - *In Vitro* Efferocytosis Assay
 - Adoptive Transfer of Treg Cells to Naive Mice
 - *Ex Vivo* Efferocytosis and Apoptotic Cell Binding Assays
 - Gene Expression Analysis
 - Gene Silencing
 - Rac1 Activity Assay

- IL-10 and IL-13 ELISAs
- Efferocytosis in Atherosclerosis
- QUANTIFICATION AND STATISTICAL ANALYSIS

SUPPLEMENTAL INFORMATION

Supplemental Information includes seven figures and one table and can be found with this article online at <https://doi.org/10.1016/j.immuni.2018.07.015>.

ACKNOWLEDGMENTS

The authors thank Dr. Andrew McKenzie of the Medical Research Council for his generous donation of the *Il13*^{-/-} mice used in this study. This work was supported by NIH T32 post-doctoral training grant HL007343 (J.D.P. and A.Y.), American Heart Association Fellow-to-Faculty Transition Awards (A.C.D. and J.H.), a grant from the Scientific and Technological Research Council of Turkey (TUBITAK), a grant from the BIDEB 2214/A Program (E.S.), a Grant-in-Aid from the American Heart Association (M.N.I.), a Stony Wold-Herbert Fund Inc. Research Fellowship (J.H.), and NIH grants HL122730 and DoD-PR150672 (J.B.) and HL132412, HL075662, and HL127464 (I.T.). These studies used the resources of the Columbia Diabetes and Endocrinology Research Center and Columbia Cancer Center flow core facilities, funded in part through NIH center grants 5P30DK063608 and P30CA013696, respectively.

AUTHOR CONTRIBUTIONS

J.D.P. and A.C.D. designed and performed experiments, collected and analyzed data, and wrote the manuscript; G.G., A.Y., E.S., M.S., M.N.I., and J.H. contributed to the experimental design and performed experiments; C.C.R., J.D., and G.K. assisted in performing experiments and data collection; J.B. contributed to the experimental design and data interpretation; and I.T. oversaw the project, designed experiments, contributed to data interpretation, and edited the manuscript.

DECLARATION OF INTERESTS

The authors declare no competing interests.

Received: October 24, 2017

Revised: April 5, 2018

Accepted: July 25, 2018

Published: October 2, 2018

REFERENCES

- Aggarwal, N.R., Tsushima, K., Eto, Y., Tripathi, A., Mandke, P., Mock, J.R., Garibaldi, B.T., Singer, B.D., Sidhaye, V.K., Horton, M.R., et al. (2014). Immunological priming requires regulatory T cells and IL-10-producing macrophages to accelerate resolution from severe lung inflammation. *J. Immunol.* *192*, 4453–4464.
- Ait-Oufella, H., Salomon, B.L., Potteaux, S., Robertson, A.K., Gourdy, P., Zoll, J., Merval, R., Esposito, B., Cohen, J.L., Fisson, S., et al. (2006). Natural regulatory T cells control the development of atherosclerosis in mice. *Nat. Med.* *12*, 178–180.
- Arandjelovic, S., and Ravichandran, K.S. (2015). Phagocytosis of apoptotic cells in homeostasis. *Nat. Immunol.* *16*, 907–917.
- Arpaia, N., Green, J.A., Moltedo, B., Arvey, A., Hemmers, S., Yuan, S., Treuting, P.M., and Rudensky, A.Y. (2015). A distinct function of regulatory T cells in tissue protection. *Cell* *162*, 1078–1089.
- Boyman, O., Kovar, M., Rubinstein, M.P., Surh, C.D., and Sprent, J. (2006). Selective stimulation of T cell subsets with antibody-cytokine immune complexes. *Science* *311*, 1924–1927.
- Buckley, C.D., Gilroy, D.W., and Serhan, C.N. (2014). Proresolving lipid mediators and mechanisms in the resolution of acute inflammation. *Immunity* *40*, 315–327.

- Cai, B., Thorp, E.B., Doran, A.C., Subramanian, M., Sansbury, B.E., Lin, C.S., Spite, M., Fredman, G., and Tabas, I. (2016). MerTK cleavage limits proresolving mediator biosynthesis and exacerbates tissue inflammation. *Proc. Natl. Acad. Sci. USA* *113*, 6526–6531.
- Cardilo-Reis, L., Gruber, S., Schreier, S.M., Drechsler, M., Papac-Milicevic, N., Weber, C., Wagner, O., Stangl, H., Soehnlein, O., and Binder, C.J. (2012). Interleukin-13 protects from atherosclerosis and modulates plaque composition by skewing the macrophage phenotype. *EMBO Mol. Med.* *4*, 1072–1086.
- Chen, H., Qin, J., Wei, P., Zhang, J., Li, Q., Fu, L., Li, S., Ma, C., and Cong, B. (2009). Effects of leukotriene B4 and prostaglandin E2 on the differentiation of murine Foxp3+ T regulatory cells and Th17 cells. *Prostaglandins Leukot. Essent. Fatty Acids* *80*, 195–200.
- Chung, E.Y., Liu, J., Homma, Y., Zhang, Y., Brendolan, A., Saggese, M., Han, J., Silverstein, R., Sella, L., and Ma, X. (2007). Interleukin-10 expression in macrophages during phagocytosis of apoptotic cells is mediated by homeodomain proteins Pbx1 and Prep-1. *Immunity* *27*, 952–964.
- D'Alessio, F.R., Tsushima, K., Aggarwal, N.R., West, E.E., Willett, M.H., Britos, M.F., Pipeling, M.R., Brower, R.G., Tuder, R.M., McDyer, J.F., and King, L.S. (2009). CD4+CD25+Foxp3+ Tregs resolve experimental lung injury in mice and are present in humans with acute lung injury. *J. Clin. Invest.* *119*, 2898–2913.
- Dinh, T.N., Kyaw, T.S., Kanellakis, P., To, K., Tipping, P., Toh, B.H., Bobik, A., and Agrotis, A. (2012). Cytokine therapy with interleukin-2/anti-interleukin-2 monoclonal antibody complexes expands CD4+CD25+Foxp3+ regulatory T cells and attenuates development and progression of atherosclerosis. *Circulation* *126*, 1256–1266.
- Fadok, V.A., Bratton, D.L., Konowal, A., Freed, P.W., Westcott, J.Y., and Henson, P.M. (1998). Macrophages that have ingested apoptotic cells in vitro inhibit proinflammatory cytokine production through autocrine/paracrine mechanisms involving TGF- β , PGE2, and PAF. *J. Clin. Invest.* *101*, 890–898.
- Fichtner-Feigl, S., Kesselring, R., Martin, M., Obermeier, F., Ruemmele, P., Kitani, A., Brunner, S.M., Haimerl, M., Geissler, E.K., Strober, W., and Schlitt, H.J. (2014). IL-13 orchestrates resolution of chronic intestinal inflammation via phosphorylation of glycogen synthase kinase-3 β . *J. Immunol.* *192*, 3969–3980.
- Foks, A.C., Frodermann, V., ter Borg, M., Habets, K.L., Bot, I., Zhao, Y., van Eck, M., van Berkel, T.J., Kuiper, J., and van Puijvelde, G.H. (2011). Differential effects of regulatory T cells on the initiation and regression of atherosclerosis. *Atherosclerosis* *218*, 53–60.
- Freire-de-Lima, C.G., Xiao, Y.Q., Gardai, S.J., Bratton, D.L., Schiemann, W.P., and Henson, P.M. (2006). Apoptotic cells, through transforming growth factor- β , coordinately induce anti-inflammatory and suppress pro-inflammatory eicosanoid and NO synthesis in murine macrophages. *J. Biol. Chem.* *281*, 38376–38384.
- Gagliani, N., Amezcuca Vesely, M.C., Iseppon, A., Brockmann, L., Xu, H., Palm, N.W., de Zoete, M.R., Licona-Limón, P., Paiva, R.S., Ching, T., et al. (2015). Th17 cells transdifferentiate into regulatory T cells during resolution of inflammation. *Nature* *523*, 221–225.
- George, J., Schwartzberg, S., Medvedovsky, D., Jonas, M., Charach, G., Afek, A., and Shamiss, A. (2012). Regulatory T cells and IL-10 levels are reduced in patients with vulnerable coronary plaques. *Atherosclerosis* *222*, 519–523.
- Godson, C., Mitchell, S., Harvey, K., Petasis, N.A., Hogg, N., and Brady, H.R. (2000). Cutting edge: Lipoxins rapidly stimulate nonphlogistic phagocytosis of apoptotic neutrophils by monocyte-derived macrophages. *J. Immunol.* *164*, 1663–1667.
- Hutchins, A.P., Poulain, S., and Miranda-Saavedra, D. (2012). Genome-wide analysis of STAT3 binding in vivo predicts effectors of the anti-inflammatory response in macrophages. *Blood* *119*, e110–e119.
- Ip, W.K.E., Hoshi, N., Shouval, D.S., Snapper, S., and Medzhitov, R. (2017). Anti-inflammatory effect of IL-10 mediated by metabolic reprogramming of macrophages. *Science* *356*, 513–519.
- Kambayashi, T., Jacob, C.O., and Strassmann, G. (1996). IL-4 and IL-13 modulate IL-10 release in endotoxin-stimulated murine peritoneal mononuclear phagocytes. *Cell. Immunol.* *171*, 153–158.
- Liu, Y., Li, D., Chen, J., Xie, J., Bandyopadhyay, S., Zhang, D., Nemarkommula, A.R., Liu, H., Mehta, J.L., and Hermonat, P.L. (2006). Inhibition of atherosclerosis in LDLR knockout mice by systemic delivery of adeno-associated virus type 2-hIL-10. *Atherosclerosis* *188*, 19–27.
- Matute-Bello, G., Downey, G., Moore, B.B., Groshong, S.D., Matthay, M.A., Slutsky, A.S., and Kuebler, W.M.; Acute Lung Injury in Animals Study Group (2011). An official American Thoracic Society workshop report: features and measurements of experimental acute lung injury in animals. *Am. J. Respir. Cell Mol. Biol.* *44*, 725–738.
- Michalski, M.N., Koh, A.J., Weidner, S., Roca, H., and McCauley, L.K. (2016). Modulation of osteoblastic cell efferocytosis by bone marrow macrophages. *J. Cell. Biochem.* *117*, 2697–2706.
- Michlewska, S., Dransfield, I., Megson, I.L., and Rossi, A.G. (2009). Macrophage phagocytosis of apoptotic neutrophils is critically regulated by the opposing actions of pro-inflammatory and anti-inflammatory agents: key role for TNF- α . *FASEB J.* *23*, 844–854.
- Mondal, S., Ghosh-Roy, S., Loison, F., Li, Y., Jia, Y., Harris, C., Williams, D.A., and Luo, H.R. (2011). PTEN negatively regulates engulfment of apoptotic cells by modulating activation of Rac GTPase. *J. Immunol.* *187*, 5783–5794.
- Neill, D.R., Wong, S.H., Bellosi, A., Flynn, R.J., Daly, M., Langford, T.K., Bucks, C., Kane, C.M., Fallon, P.G., Pannell, R., et al. (2010). Neutrophils represent a new innate effector leukocyte that mediates type-2 immunity. *Nature* *464*, 1367–1370.
- Newson, J., Stables, M., Karra, E., Arce-Vargas, F., Quezada, S., Motwani, M., Mack, M., Yona, S., Audzevich, T., and Gilroy, D.W. (2014). Resolution of acute inflammation bridges the gap between innate and adaptive immunity. *Blood* *124*, 1748–1764.
- Ochoa-Repáraz, J., Rynda, A., Ascón, M.A., Yang, X., Kochetkova, I., Riccardi, C., Callis, G., Trunkle, T., and Pascual, D.W. (2008). IL-13 production by regulatory T cells protects against experimental autoimmune encephalomyelitis independently of autoantigen. *J. Immunol.* *181*, 954–968.
- Ogden, C.A., Pound, J.D., Bath, B.K., Owens, S., Johannessen, I., Wood, K., and Gregory, C.D. (2005). Enhanced apoptotic cell clearance capacity and B cell survival factor production by IL-10-activated macrophages: implications for Burkitt's lymphoma. *J. Immunol.* *174*, 3015–3023.
- Pinderski, L.J., Fischbein, M.P., Subbanagounder, G., Fishbein, M.C., Kubo, N., Cheroutre, H., Curtiss, L.K., Berliner, J.A., and Boisvert, W.A. (2002). Overexpression of interleukin-10 by activated T lymphocytes inhibits atherosclerosis in LDL receptor-deficient Mice by altering lymphocyte and macrophage phenotypes. *Circ. Res.* *90*, 1064–1071.
- Pottea, S., Esposito, B., van Oostrom, O., Brun, V., Ardouin, P., Groux, H., Tedgui, A., and Mallat, Z. (2004). Leukocyte-derived interleukin 10 is required for protection against atherosclerosis in low-density lipoprotein receptor knockout mice. *Arterioscler. Thromb. Vasc. Biol.* *24*, 1474–1478.
- Ravichandran, K.S., and Lorenz, U. (2007). Engulfment of apoptotic cells: Signals for a good meal. *Nat. Rev. Immunol.* *7*, 964–974.
- Saito, M., Iwakaki, T., Taya, C., Yonekawa, H., Noda, M., Inui, Y., Mekada, E., Kimata, Y., Tsuru, A., and Kohno, K. (2001). Diphtheria toxin receptor-mediated conditional and targeted cell ablation in transgenic mice. *Nat. Biotechnol.* *19*, 746–750.
- Schindelin, J., Arganda-Carreras, I., Frise, E., Kaynig, V., Longair, M., Pietzsch, T., Preibisch, S., Rueden, C., Saalfeld, S., Schmid, B., et al. (2012). Fiji: An open-source platform for biological-image analysis. *Nat. Methods* *9*, 676–682.
- Schmidt, E.P., and Tuder, R.M. (2010). Role of apoptosis in amplifying inflammatory responses in lung diseases. *J. Cell Death* *2010*, 41–53.
- Schrijvers, D.M., De Meyer, G.R., Kockx, M.M., Herman, A.G., and Martinet, W. (2005). Phagocytosis of apoptotic cells by macrophages is impaired in atherosclerosis. *Arterioscler. Thromb. Vasc. Biol.* *25*, 1256–1261.
- Schust, J., Sperl, B., Hollis, A., Mayer, T.U., and Berg, T. (2006). Stattic: A small-molecule inhibitor of STAT3 activation and dimerization. *Chem. Biol.* *13*, 1235–1242.

- Serhan, C.N., Chiang, N., Dalli, J., and Levy, B.D. (2014). Lipid mediators in the resolution of inflammation. *Cold Spring Harb. Perspect. Biol.* 7, a016311.
- Spencer, S.D., Di Marco, F., Hooley, J., Pitts-Meek, S., Bauer, M., Ryan, A.M., Sordat, B., Gibbs, V.C., and Aguet, M. (1998). The orphan receptor CRF2-4 is an essential subunit of the interleukin 10 receptor. *J. Exp. Med.* 187, 571–578.
- Subramanian, M., Thorp, E., Hansson, G.K., and Tabas, I. (2013). Treg-mediated suppression of atherosclerosis requires MYD88 signaling in DCs. *J. Clin. Invest.* 123, 179–188.
- Subramanian, M., Hayes, C.D., Thome, J.J., Thorp, E., Matsushima, G.K., Herz, J., Farber, D.L., Liu, K., Lakshmana, M., and Tabas, I. (2014). An AXL/LRP-1/RANBP9 complex mediates DC efferocytosis and antigen cross-presentation in vivo. *J. Clin. Invest.* 124, 1296–1308.
- Sutmoller, R.P., van Duivenvoorde, L.M., van Elsas, A., Schumacher, T.N., Wildenberg, M.E., Allison, J.P., Toes, R.E., Offringa, R., and Melief, C.J. (2001). Synergism of cytotoxic T lymphocyte-associated antigen 4 blockade and depletion of CD25(+) regulatory T cells in antitumor therapy reveals alternative pathways for suppression of autoreactive cytotoxic T lymphocyte responses. *J. Exp. Med.* 194, 823–832.
- Thorp, E., Cui, D., Schrijvers, D.M., Kuriakose, G., and Tabas, I. (2008). Merck receptor mutation reduces efferocytosis efficiency and promotes apoptotic cell accumulation and plaque necrosis in atherosclerotic lesions of *apoe*^{-/-} mice. *Arterioscler. Thromb. Vasc. Biol.* 28, 1421–1428.
- Tziakas, D.N., Chalikias, G.K., Kaski, J.C., Kekes, A., Hatzinikolaou, E.I., Stakos, D.A., Tentis, I.K., Kortsaris, A.X., and Hatseras, D.I. (2007). Inflammatory and anti-inflammatory variable clusters and risk prediction in acute coronary syndrome patients: a factor analysis approach. *Atherosclerosis* 193, 196–203.
- Weirather, J., Hofmann, U.D., Beyersdorf, N., Ramos, G.C., Vogel, B., Frey, A., Ertl, G., Kerkau, T., and Frantz, S. (2014). Foxp3+ CD4+ T cells improve healing after myocardial infarction by modulating monocyte/macrophage differentiation. *Circ. Res.* 115, 55–67.
- Yurdagul, A., Jr., Doran, A.C., Cai, B., Fredman, G., and Tabas, I.A. (2018). Mechanisms and consequences of defective efferocytosis in atherosclerosis. *Front. Cardiovasc. Med.* 4, 86.

STAR★METHODS

KEY RESOURCES TABLE

REAGENT or RESOURCE	SOURCE	IDENTIFIER
Antibodies		
Aqua-fixable LIVE/DEAD stain	Thermo Fisher	Cat# L24957
Goat anti-IL-13 (neutralizing antibody, <i>in vitro</i> use)	R&D Systems	Cat# AF-413-NA; RRID: AB_2124173
Hamster anti-CD11c (clone N418)	Biolegend	Cat# 117323; RRID: AB_830646
Hamster anti-CD3 (clone 145-2C11), purified	BD Biosciences	Cat# 553058; RRID: AB_394591
Hamster anti-CD25 (clone 37.51), purified	BD Biosciences	Cat# 553295; RRID: AB_394764
Mouse anti-phospho-(Y705)-STAT3 (clone LUVNKLA)	eBioscience	Cat# 12-9033-42; RRID: AB_2572679
Mouse anti-STAT3 (clone M59-50)	BD Biosciences	Cat# 560392; RRID: AB_1645463
Rat anti-CD3 (clone 17A2)	BD Biosciences	Cat# 564009; RRID: AB_2732063
Rat anti-CD4 (clone GK1.5)	eBioscience	Cat# 17-0041-82; RRID: AB_469320
Rat anti-CD11b (clone M1/70)	eBioscience	Cat# 101215; RRID: AB_312798
Rat anti-IL-2 (clone JES6-1A12)	R&D Systems	Cat# MAB702; RRID: AB_2123681
Rat anti-IL-10 (clone JES5-2A5, neutralizing antibody for <i>in vivo</i> use)	BioXCell	Cat# BE0049; RRID: AB_1107696
Rat anti-IL-13 (clone 1316H, neutralizing antibody for <i>in vivo</i> use)	eBioscience	Cat# 16-7135-85; RRID: AB_763563
Rat anti-CD16/CD32 (clone 93)	Biolegend	Cat# 101302; RRID: AB_312801
Rat anti-CD25 (clone PC-61.5.3) – for <i>in vivo</i> use	BioXCell	Cat# BE0012; RRID: AB_1107619
Rat anti-CD25 (eBio7D4) – for flow cytometry use	eBioscience	Cat# 53-0252-82; RRID: AB_763470
Rat anti-CD170 (SiglecF, clone 1RNM44N)	eBioscience	Cat# 46-1702-82; RRID: AB_2573724
Rat anti-F4/80 (clone BM8)	Biolegend	Cat# 123108; RRID: AB_893502
Rat anti-Foxp3 (clone FJK-16 s)	eBioscience	Cat# 12-5773-80; RRID: AB_465935
Rat anti-Mac3 (clone M3/84)	BD Biosciences	Cat# 553322; RRID: AB_394780
Rat IgG (companion to rat anti-IL-13 above)	eBioscience	Cat# 16-4301-85; RRID: AB_470154
Rat IgG (companion to rat anti-IL-10 above)	BioXCell	Cat# BE0088; RRID: AB_1107775
Goat anti-rabbit secondary antibody (AlexaFluor 647)	Sigma-Aldrich	Cat# SAB4600184; RRID: AB_2665437
Goat anti-rabbit secondary antibody (AlexaFluor 488)	Invitrogen	Cat# A11008; RRID: AB_143165
Chemicals, Peptides, and Recombinant Proteins		
CellStripper	Corning	Cat# 25-056-CI
Dulbecco's Modified Eagle Medium (DMEM)	Corning	Cat# 10-013-CV
Diphtheria Toxin	Sigma-Aldrich	Cat# D0564
Fix/Perm Buffer	eBioscience	Cat# 00-523-43
GM-CSF	Peptotech	Cat# 300-03
Heat-Inactivated Fetal Bovine Serum	GIBCO	Cat# 10438-026
IL-2, mouse	Peptotech	Cat# 212-12
IL-10, mouse	Peptotech	Cat# 210-10
IL-10, human	Peptotech	Cat# 200-10
IL-13, mouse	Peptotech	Cat# 210-3
Liberase TL	Sigma/Roche	Cat# 05401020001
Lipofectamine RNAi Max	Invitrogen	Cat# 13778
Lipopolysaccharide (LPS)	Sigma-Aldrich	Cat# L4130
Lymphoprep	Stem Cell Technologies	Cat# 07801
Penicillin/Streptomycin	Corning	Cat# 30-002-CI
Permeabilization Buffer	eBioscience	Cat# 00-8333-56
Phosphate Buffered Saline, 1X	Corning	Cat# 21-040-CV
PKH67 Fluorescent Cell Linker	Sigma-Aldrich	Cat# PKH67GL-1KT
Polystyrene beads, 4 μ m	Thermo Fisher	Cat# F8858

(Continued on next page)

Continued

REAGENT or RESOURCE	SOURCE	IDENTIFIER
Power SYBR Green PCR Master Mix	Applied Biosystems	Cat# 4367659
Protease and Proteinase Inhibitor Cocktail	Thermo Fisher	Cat# 78446
Proteinase K	Dako	Cat# S3020
Red Blood Cell Lysis Buffer	Sigma-Aldrich	Cat# R7757
Radioimmunoprecipitation (RIPA) buffer	Santa Cruz	Cat# sc-24948
Sepmate conical tubes	Stem Cell Technologies	Cat# 85450
Zymosan A	Sigma-Aldrich	Cat# Z4250
Critical Commercial Assays		
EasySep Mouse CD4 ⁺ T cell Enrichment Kit	Stem Cell Technologies	Cat# 19852
EasySep Mouse CD25 ⁺ T cell Enrichment Kit	Stem Cell Technologies	Cat# 18782
EasySep Mouse Neutrophil Enrichment Kit	Stem Cell Technologies	Cat #19762
G-LISA Rac1 Activation Assay Kit	Cytoskeleton	Cat# BK128
IL-10 ELISA	R&D Systems	Cat# M1000B
IL-13 ELISA	R&D Systems	Cat# M1300CB
Maxima First Strand cDNA Synthesis Kit	Thermo Fisher	Cat# K1671
Precision Red Protein Assay	Cytoskeleton	Cat# ADV02-A
RNeasy Isolation Kit	QIAGEN	Cat# 74106
THR Red Cell Death (TUNEL) Detection Kit	Sigma/Roche	Cat# 12156792910
Total Cholesterol Kit	Wako Diagnostics	Cat# 999-02601
Triglycerides Kit	Wako Diagnostics	Cat# 994-02891
Experimental Models: Cell Lines		
Human: Jurkat cells	ATCC	ATCC TIB-152; RRID: CVCL_0367
Mouse: L-929 Fibroblast cells	ATCC	ATCC CCL-1; RRID: CVCL_0462
Mouse: Bone-Marrow-Derived Macrophage cells	This paper	N/A
Mouse: Elicited Peritoneal Macrophage cells	This paper	N/A
Human: Peripheral Blood Monocyte-Derived Macrophage cells	This paper	N/A
Experimental Models: Organisms/Strains		
Mouse: C57BL/6J (WT)	Jackson Laboratories	Stock# 000664; RRID: IMSR_JAX:000664
Mouse: B6.129S7-Ldlr ^{tm1Her} /J (<i>Ldlr</i> ^{-/-})	Jackson Laboratories	Stock# 002207; RRID: IMSR_JAX:002207
Mouse: B6.129P2-Il10 ^{tm1Cgn} /J (<i>Il10</i> ^{-/-})	Jackson Laboratories	Stock# 002251; RRID: IMSR_JAX:002251
Mouse: B6.129S2-Il10rb ^{tm1Agt} /J (<i>Il10rb</i> ^{-/-})	Jackson Laboratories	Stock# 005027; RRID: IMSR_JAX:005027
Mouse: B6.129(Cg)-Foxp3 ^{tm3(DTR/GFP)Ayr} /J (hDTR-Foxp3)	Jackson Laboratories	Stock# 016958; RRID: IMSR_JAX:016958
Mouse: <i>Il13</i> ^{eGFP}	Neill et al., 2010	N/A
Oligonucleotides		
ON-TARGET plus non-targeting pool	GE Dharmacon	Cat# D-001810-10
IL-13 SMART pool	GE Dharmacon	Cat# L-046599-01
Vav1 SMART pool	GE Dharmacon	Cat# L-065359-01
For primer information, please refer to Table S1	N/A	N/A
Software and Algorithms		
BD FACSDIVA	BD Biosciences	N/A
Fiji	Schindelin et al., 2012	http://www.fiji.sc
FlowJo	FlowJo	Version 10
ImageJ	NIH	http://www.imagej.nih.gov/ij
ImagePro Plus	Media Cybernetics	N/A
Leica Application Suite	Leica	Advanced fluoroscope
Prism	Graph Pad	Version 7

(Continued on next page)

Continued

REAGENT or RESOURCE	SOURCE	IDENTIFIER
Other		
Amicon Ultra 3K centrifugal filter units	Millipore	Cat# UFC500324
Genotyping Service	Genetyper	http://www.genetyper.com
Microhematocrit microcapillary tubes	Thermo Fisher	Cat# 22-362-566
Mouse diet: high-fat Western diet	Envigo	Cat# TD.88137

CONTACT FOR REAGENT AND RESOURCE SHARING

Further information and requests for resources and reagents should be directed to and will be fulfilled by the Lead Contact, Dr. Ira Tabas (iat1@cumc.columbia.edu). An MTA was obtained for the transfer of *I13^{-/-}* mice.

EXPERIMENTAL MODEL AND SUBJECT DETAILS

Cell Lines

Jurkat (human T lymphocytes) and L-929 (mouse fibroblasts) cells were maintained in Dulbecco's modified Eagle's medium (DMEM) supplemented with 10% (vol/vol) heat-inactivated fetal bovine serum (HI-FBS), and 10 U/mL penicillin and 100 µg/mL streptomycin. Cells were cultured in a humidified CO₂ incubator at 37°C.

Primary Cell Cultures

For bone marrow-derived macrophages (BMDMs), bone marrow cells from 8-12 week old male or female mice were cultured in DMEM supplemented with 10% (vol/vol) heat-inactivated FBS, 10 U/mL penicillin, 100 µg/mL streptomycin, and 20% (vol/vol) L-929 fibroblast-cultured media supernatants for 7-9 days (Thorp et al., 2008). For human macrophages, buffy coats were purchased from the New York Blood Donor Center, and peripheral blood mononuclear cells (PBMCs) were isolated using Lymphoprep according to the manufacturer's instructions. Briefly, Lymphoprep was added to the bottom of 50-mL Sepmate conical tubes, and buffy coat (diluted 1:1 with PBS containing 2% FBS) was layered above. Tubes were centrifuged at 800 × *g* for 20 min at room temperature to collect the mononuclear cell fraction. Approximately 60 million PBMCs were plated on 10-cm Petri dishes. After 1 hr, non-adherent cells were removed by washing, and the adherent cells were cultured with Roswell Park Memorial Institute 1640 media (RPMI-1640) supplemented with 10% FBS and 10 ng/mL recombinant human GM-CSF for 7 days, with the medium replaced after the first 3 days. Columbia University Institutional Review Board and Health Insurance Portability and Accountability Act guidelines were followed for isolating peripheral human blood monocytes.

Experimental Animals

Animal protocols were approved by Columbia University's Institutional Animal Care and Use Committee. All animals were cared for according to the NIH guidelines for the care and use of laboratory animals. Mice were socially housed under a 12-hour light-dark cycle with *ad libitum* access to water and food. All mice were on the C57BL/6J background. C57BL/6J (WT), B6.129S7-*Ldlr^{tm1Her}/J* (*Ldlr^{-/-}*), B6.129P2-*Il10^{tm1Cgn}/J* (*Il10^{-/-}*), B6.129S2-*Il10rb^{tm1Agt}/J* (*Il10rb^{-/-}*), B6.129(Cg)-*Foxp3^{tm3(DTR/GFP)Ayr}/J*, and B6.129S7-*Rag1^{tm1Mom}/J* (*Rag1^{-/-}*) mice were purchased from Jackson Laboratories. *I13^{-/-}* mice were a generous gift from Andrew McKenzie at the MRC Laboratory of Molecular Biology in Cambridge, UK (Neill et al., 2010). Male and female mice between the ages of 8-20 weeks were used in this study, and all mice were assigned randomly to the various experimental groups.

METHOD DETAILS

Zymosan-Induced Peritonitis

Peritonitis was induced by i.p. injection of 0.1 mg zymosan A in a 500 µL volume per mouse (day 0). Treg cells were depleted in *Foxp3*-human DTR mice by i.p. injection of diphtheria toxin at day 4 (50 µg/kg), day 6 (15 µg/kg), and day 8 (15 µg/kg). Mice were sacrificed on day 11, and peritoneal exudates were collected by lavage with 2 mL of sterile PBS.

Peritoneal Uptake of Labeled Apoptotic Cells (ACs)

Neutrophils were collected by peritoneal lavage from donor mice 6 hr after they had been injected with 1 mg of zymosan A. The lavage fluid was passed through a 40-µm strainer and washed, and neutrophils were isolated with the EasySep Mouse Neutrophil Enrichment Kit according to manufacturer's instructions and then cultured overnight in medium containing 1% FBS and 1% penicillin and streptomycin in DMEM. On the following day, the neutrophils, which were now apoptotic, were labeled with PKH26 red according to the manufacturer's instructions. The recipient mice were injected i.p. with 4 × 10⁶ of these labeled apoptotic cells, and 45 min later, the mice were sacrificed and the peritoneum was lavaged. Efferocytosis was quantified as the percentage of F4/80⁺ macrophages that had taken up one or more PKH-labeled apoptotic cells.

Acute Lung Injury

LPS (3.75 $\mu\text{g/g}$ body weight) was delivered by intranasal installation (day 0). To deplete Treg cells in DT-Treg cell mice, 50 $\mu\text{g/kg}$ body weight diphtheria toxin was delivered i.p. at day 1. Alternatively, Treg cells were depleted in WT mice by injection of 0.5 mg anti-CD25 antibody at days -2 and $+1$. For cells in which Treg cells were administered to mice, 2×10^6 cells were resuspended in 40 μL of PBS and delivered intranasally to anesthetized mice. Four days post-LPS, mice were sacrificed, blood was removed by cardiac puncture, and the vasculature was perfused with PBS. Lungs were either lavaged with PBS, fixed by gravity perfusion of formalin, or harvested, minced, and digested with Liberase TL for 30 min at 37°C , followed by staining for flow cytometry. For 7-day experiments, mice were given additional doses of diphtheria toxin (15 $\mu\text{g/kg}$ body weight) at days 3 and 5 post-LPS.

Lung Histology

Formalin-fixed lung tissues were paraffin-embedded and then sectioned. Tissue sections were stained with hematoxylin and eosin, then examined and quantitatively analyzed using a Nikon Labphoto 2 microscope equipped with Image Pro Plus software. Injury scoring was conducted by a blinded observer according to a previously established method (Matute-Bello et al., 2011). Briefly, images were scored for neutrophil localization to the alveolar and interstitial spaces, as well as the presence of air space debris and alveolar septal thickening.

In Situ Efferocytosis Analysis

Efferocytosis was determined using previously described methods (Thorp et al., 2008). Apoptotic cells were identified in tissue sections by performing terminal deoxynucleotidyl transferase dUTP nick end labeling (TUNEL) using the tetramethylrhodamine red *in situ* cell death detection kit according to the manufacturer's protocols. Frozen tissues were first fixed with ice-cold acetone for 3 min at -20°C . In the case of formalin-fixed paraffin embedded tissues, tissues were first deparaffinized and incubated with proteinase K solution according to the manufacturer's instructions. Following TUNEL staining, sections were incubated with primary antibodies against Mac3 or F4/80, and then by Alexa Fluor 647- or Alex Fluor 488-conjugated secondary antibodies to identify macrophages. Images were captured using a Leica DMI 6000B or an Olympus IX-70 microscope and analyzed using ImageJ software. Briefly, the number of apoptotic cells that co-localized with or were adjacent to macrophages ("associated") and those that were not associated with macrophages ("free") were counted. Efferocytosis efficiency was quantified based on the ratio of associated:free apoptotic cells per tissue section.

Flow Cytometry

Cells were washed, resuspended in staining buffer consisting of 2% FBS in PBS with 2 mM EDTA, blocked with anti-mouse CD16/32 antibodies for 10 min, and then incubated with primary antibodies. Treg cells in bronchoalveolar lavage samples from *Foxp3^{GFP/DTR}* mice were identified by first immunostaining for CD4 or CD3 and then by assaying eGFP expression among these cells. To analyze splenic T cells, spleens were processed to form a single-cell suspension and then placed through a 40- μm filter. Following red blood cell lysis, cells were blocked and stained for CD4 and CD25. Alternatively, following surface staining, cells were incubated with fixation-permeabilization buffer, washed with permeabilization buffer, and then incubated with Foxp3 antibody. Peripheral blood samples were collected after tail clipping using microhematocrit microcapillary tubes. Circulating Treg cells were then analyzed in a similar manner to splenic Treg cells. To analyze lung macrophages, cells were incubated with aqua-fixable LIVE-DEAD stain according to the manufacturer's protocol and then immunostained for CD11b, Siglec F, F4/80, and CD11c. For phospho-STAT3 flow cytometry, cells were fixed with 2% paraformaldehyde for 15 min at room temperature, permeabilized with 0.2% tween-20 for 10 min at room temperature, washed with permeabilization buffer, and then incubated with phospho-(Y705)-STAT3 antibody, and, in some cases, also total STAT3 antibody. Samples were processed on a BD FACSCanto II or BD Fortessa and analyzed with FlowJo software.

Regulatory T Cell Isolation

Spleens were collected from WT, *Il10^{-/-}*, or *Il13^{-/-}* mice and processed into a single cell suspension. CD4⁺ T cells were first enriched using the EasySep Mouse CD4⁺ T cell enrichment kit according to the manufacturer's instructions. CD4⁺CD25⁺ T cells were then purified using the mouse CD25 regulatory T cell positive selection kit. Purity was assessed by flow cytometry analysis and cells were typically >93% CD4⁺CD25⁺.

In Vitro Efferocytosis Assay

In vitro efferocytosis assays were performed according to established protocols (Subramanian et al., 2014). Primary bone marrow-derived macrophages were cultured at 3×10^5 cells per well in 24-well tissue culture plates. To carry out efferocytosis, macrophages were incubated for 2 hr with PKH26-labeled Jurkat cells that were rendered apoptotic by UV-irradiation (Subramanian et al., 2014) at a ratio of 5:1 apoptotic cells: macrophage. Cultures were then vigorously washed, and fluorescence and bright field images were taken on an Olympus IX-70 microscope to identify uptake of labeled cells. Images were quantified using ImageJ software. A similar protocol was used to assay efferocytosis by human monocyte-derived macrophages. In the case of macrophage and Treg cell co-cultures, Treg cells were isolated as described above and then cultured with macrophages for ~ 40 hr at a ratio of 1:4 (Treg cell:macrophage) in the presence of anti-CD3 (62.5 ng/mL). For rIL-10 or rIL-13 treatment, macrophages were exposed

to recombinant mouse IL-10 or IL-13 at the indicated dose for 48 hr prior to efferocytosis assays. To neutralize IL-13, an IL-13 neutralizing antibody (5 $\mu\text{g}/\text{mL}$) was added to the culture media during co-culture.

Adoptive Transfer of Treg Cells to Naive Mice

Treg cells were isolated from the spleens of donor WT, *IL10*^{-/-}, or *IL-13*^{-/-} mice as described above. For peritonitis studies, recipient mice were injected i.p. with 5×10^5 Treg cells. Three days later, mice were sacrificed and the peritoneal cavity was lavaged to collect resident macrophages. For IL-13 neutralization studies, mice were co-injected with either IgG (200 μg) or IL-13 neutralizing antibody (200 μg). For lung injury studies in which Treg cells were administered to mice, $0.75\text{--}2 \times 10^6$ Treg cells were resuspended in 40 μL of PBS and delivered intranasally to anesthetized mice.

Ex Vivo Efferocytosis and Apoptotic Cell Binding Assays

Peritoneal lavage cells were collected from mice and plated on 24-well plates. After 2 hr, the medium was aspirated and the cells were washed. The remaining adherent cells were >90% F4/80⁺ macrophages. Efferocytosis was carried out as described above. To measure apoptotic cell binding capacity, plates were incubated at 4°C for 1 hr immediately after the addition of labeled apoptotic Jurkat cells. Plates were washed with cold PBS and then imaged as described above.

Gene Expression Analysis

RNA was isolated using the RNeasy Isolation kit and reverse transcribed using the Maxima First strand cDNA synthesis kit (Thermo Fisher Scientific, K1671) according to the manufacturer's protocol. RT-PCR was conducted on a 7500 Realtime PCR system (Applied Biosystems) using Power SYBR Green master mix (Thermo Fisher Scientific, 4367659). For primer sequences, please see [Table S1](#).

Gene Silencing

Macrophages were transfected with ON-TARGETplus SMARTpool siRNA against Vav1 (15 nM) or IL-13 (30 nM) using Lipofectamine RNAiMax reagent according to the manufacturer's instructions. Gene silencing was evaluated by RT-PCR.

Rac1 Activity Assay

Macrophages were plated on 12-well plates and exposed to 4- μm polystyrene beads at a macrophage:bead ratio of 1:5. The cells were then washed thoroughly and lysed with RIPA buffer containing Halt protease and phosphatase inhibitor cocktail. Protein concentrations were determined using the precision red protein assay. Rac1 activity was determined using the G-LISA Rac1 activation assay kit, according to the manufacturer's instructions.

IL-10 and IL-13 ELISAs

To assay IL-10 and IL-13 in the conditioned medium of cultured Treg cells, a 48-well cell culture plate was coated with 200 $\mu\text{L}/\text{well}$ purified CD3 and incubated overnight at 4°C. Treg cells were isolated as above and resuspended at a density of 1×10^6 cells per 500 μL of DMEM media containing 10% FBS and penicillin and streptomycin. Certain samples also included CD28 (2 $\mu\text{g}/\text{mL}$) and/or IL-2 (10 ng/mL). Treg cells were then plated at 1×10^6 and incubated overnight at 37°C and 5% CO₂. Conditioned media were then collected from the wells, pelleted in order to get rid of cells, and concentrated approximately 4-fold using Amicon Ultra 3K centrifugal filter units. 50 μL aliquots of these concentrated Treg cell-conditioned medium samples were assayed in duplicate using commercially available IL-10 ELISA or IL-13 ELISA kits according to the manufacturer's instructions. To assay IL-10 and IL-13 in peritoneal exudates, the peritoneums of mice were lavaged with 2ml of cold PBS. Exudates were centrifuged and the pellet was saved for further analyses. The exudate was then concentrated approximately 8-fold using Amicon Ultra 3K centrifugal filter units. 50 μL aliquots of these concentrated Treg cell-conditioned medium samples were assayed IL-10 or IL-13 as above.

Efferocytosis in Atherosclerosis

Beginning at approximately 10 weeks of age, *Ldlr*^{-/-} mice were fed a saturated fat and cholesterol-containing WD *ad libitum* for 12 weeks, leading to advanced atherosclerosis. At this time, the mice were divided into four treatment groups: IgG only (control), IL-2 complex and IgG, and IL-2 complex and anti-IL-10, and anti-IL-10 alone. Rat IgG or anti-IL-10 antibody was administered twice weekly i.p. in 200- μg doses. IL-2 complexes were formed as previously described ([Foks et al., 2011](#)). Briefly, each dose per mouse consisted of 1 μg of recombinant IL-2 that had been incubated with 5 μg of IL-2 antibody for 30 min at 37°C in PBS. Mice were administered IL-2 complex i.p. for 3 consecutive days and then once every 5 days thereafter for the duration of the 3-week treatment period. Mice remained on WD during this time, such that at the time of sacrifice, the mice had been fed the WD for 15 weeks. Following completion of the WD-feeding period, mice were euthanized using isoflurane inhalation followed by exsanguination via cardiac puncture. The heart with the aortic root attached was harvested, embedded in OCT medium, and frozen on dry ice. Aortic root sections were prepared using a cryomicrotome and then stained with hematoxylin and eosin. Images were captured on a Nikon Labphoto 2 microscope and analyzed with Image Pro Plus analysis software and analyzed as described previously ([Subramanian et al., 2013](#)). Total plasma cholesterol and triglycerides were determined using the Cholesterol E and Triglyceride M kits, respectively, according to the manufacturer's instructions. Fasting blood glucose concentration was determined using glucose test strips and a One Touch Ultra glucometer.

QUANTIFICATION AND STATISTICAL ANALYSIS

Data were tested for normality using the Kolmogorov-Smirnov test, and statistical significance was determined using GraphPad Prism software. Data that passed the normality were analyzed using Student's t test for two groups with one variable tested and equal variances, one-way ANOVA with Tukey's post-test for multiple groups with only variable tested, or two-way ANOVA with Sidak's post-tests for more than two groups with multiple variables tested. Data that were not normally distributed but contained equal variances were analyzed using the nonparametric Mann-Whitney U test with post hoc analysis. Data are shown as mean values \pm SEM. Differences were considered statistically significant at $p < 0.05$.